Since January 2020 Elsevier has created a COVID-19 resource centre with free information in English and Mandarin on the novel coronavirus COVID-19. The COVID-19 resource centre is hosted on Elsevier Connect, the company's public news and information website.

Bioorganic Chemistry 135 (2023) 106390

Contents lists available at ScienceDirect

Bioorganic Chemistry

journal homepage: www.elsevier.com/locate/bioorg

Green and efficient one-pot three-component synthesis of novel drug-like furo[2,3-*d*]pyrimidines as potential active site inhibitors and putative allosteric hotspots modulators of both SARS-CoV-2 M^{Pro} and PL^{Pro}

Hossein Mousavi [a,*], Behzad Zeynizadeh [a], Mehdi Rimaz [b]

[a] Department of Organic Chemistry, Faculty of Chemistry, Urmia University, Urmia, Iran
[b] Department of Chemistry, Payame Noor University, P.O. Box 19395-3697, Tehran, Iran

ARTICLE INFO

Keywords:
COVID-19
SARS-CoV-2
Main protease (M^{Pro})
Papain-like protease (PL^{Pro})
Multi-targeting inhibitor
Molecular docking
ADMET
Green chemistry
One-pot
Multi-component reaction (MCR)
Furo[2,3-*d*]pyrimidine

ABSTRACT

In this paper, an environmentally benign, convenient, and efficient one-pot three-component reaction has been developed for the regioselective synthesis of novel 5-aroyl(or heteroaroyl)-6-(alkylamino)-1,3-dimethylfuro[2,3-*d*]pyrimidine-2,4(1*H*,3*H*)-diones (**4a–n**) through the sequential condensation of aryl(or heteroaryl)glyoxal monohydrates (**1a–g**), 1,3-dimethylbarbituric acid (**2**), and alkyl(viz. cyclohexyl or *tert*-butyl)isocyanides (**3a** or **3b**) catalyzed by ultra-low loading $ZrOCl_2 \bullet 8H_2O$ (just 2 mol%) in water at 50 ℃. After synthesis and characterization of the mentioned furo[2,3-*d*]pyrimidines (**4a–n**), their multi-targeting inhibitory properties were investigated against the active site and putative allosteric hotspots of both SARS-CoV-2 main protease (M^{Pro}) and papain-like protease (PL^{Pro}) based on molecular docking studies and compare the attained results with various medicinal compounds which approximately in three past years were used, introduced, and or repurposed to fight against COVID-19. Furthermore, drug-likeness properties of the mentioned small heterocyclic frameworks (**4a–n**) have been explored using *in silico* ADMET analyses. Interestingly, the molecular docking studies and ADMET-related data revealed that the novel series of furo[2,3-*d*]pyrimidines (**4a–n**), especially 5-(3,4-methylendioxybenzoyl)-6-(cyclohexylamino)-1,3-dimethylfuro[2,3-*d*]pyrimidine-2,4(1*H*,3*H*)-dione (**4g**) as hit one is potential COVID-19 drug candidate, can subject to further *in vitro* and *in vivo* studies. It is worthwhile to note that the protein–ligand-type molecular docking studies on the human body temperature-dependent M^{Pro} protein that surprisingly contains $zinc^{II}$ (Zn^{II}) ion between His41/Cys145 catalytic dyad in the active site, which undoubtedly can make new plans for designing novel SARS-CoV-2 M^{Pro} inhibitors, is performed for the first time in this paper, to the best of our knowledge.

1. Introduction

The coronavirus disease 2019 (COVID-19), which was caused by the novel severe acute respiratory syndrome coronavirus 2 (SARS-CoV-2), is a life-threatening infectious disease that has posed significant global hazard concerning, including high mortality rate, economic breakdown, life distress, etc. [1]. By end of January 2023, based on World Health Organization (WHO) coronavirus disease situation dashboard and COVID-19 Map-Johns Hopkins Coronavirus Resource Center, over 754 million people had been infected with SARS-CoV-2 worldwide, and more than 6,800,000 reported deaths globally, unfortunately. The SARS-CoV-2 main protease (M^{Pro}) [2] and papain-like protease (PL^{Pro}) [3] are the most validated antiviral drug targets for combating COVID-19 because the SARS-CoV-2 M^{Pro} and PL^{Pro} are essential for viral replication, transcription, maintenance, and its life cycle. Therefore, the design and synthesis of small organic molecules that operate simultaneously as inhibitors of both SARS-CoV-2 M^{Pro} and PL^{Pro} targets are definitely worthwhile in this era. As a matter of fact, despite remarkable efforts in the nearly past three years, the scientific community's understanding about the SARS-CoV-2 phenomenon is still so limited that caused many serious restrictions on the design and preparation of new drugs or vaccines for the combating against the mentioned viral disease, regrettably [4]. Computer-aided drug design (CADD) approaches [5], which in recent years have become an indispensable constituent in medicinal chemistry, can be unquestionably practicable in a full-scale war with COVID-19 [6]. Notably, in the drug design field,

* Corresponding author.
E-mail address: 1hossein.mousavi@gmail.com (H. Mousavi).

https://doi.org/10.1016/j.bioorg.2023.106390
Received 29 December 2022; Received in revised form 17 January 2023; Accepted 20 January 2023
Available online 28 January 2023

computational studies are free from safety and ethical constraints and can increase the speed of a pharmaceutically relevant project and intensely reduce extravagant costs.

Heterocyclic compounds are valuable organic frameworks in myriad aspects of our life, especially in medicinal chemistry [7]. Furo[2,3-*d*] pyrimidine heterocyclic fused ring systems are structural analogs of purines and have diverse biological activities. As shown in Fig. 1, some heterocyclic frameworks with the furo[2,3-*d*]pyrimidine core reported as inhibitors of epidermal growth factor receptor (EGFR) [8], activated Cdc42-associated kinase 1 (ACK-1) [9], lymphocyte-specific protein tyrosine kinase (LCK) [10], glycogen synthase kinase-3 beta (GSK-3*β*) [11], receptor-interacting serine/threonine-protein kinase 1 (RIPK-1) [12], and aurora kinase A (AK-A) [13]. Besides, Miyazaki and co-workers reported 1-(4-(4-amino-6-(4-methoxyphenyl)furo[2,3-*d*]pyrimidin-5-yl)phenyl)-3-(2-fluoro-5-(trifluoromethyl)phenyl)urea compound as dual inhibitors of thymidylate synthase (TS) and dihydrofolate reductase (DHFR) [14]. Also, Gangjee *et al.* reported (4-((2,4-diamino-5-methylfuro[2,3-*d*]pyrimidin-6-yl)thio)benzoyl)-L-glutamic acid scaffold as dual inhibitors of Tie-2 and vascular endothelial growth factor 2 (VEGFR-2) [15]. In addition, some of the mentioned compounds were reported as antifolate [16] and potent anti-breast cancer [17] agents. Because of the mentioned significant biological features and many others, which are existed in scientific papers [18], furo[2,3-*d*] pyrimidines have become an attractive synthetic target for organic and medicinal synthetic groups.

Today, it is imperative to follow green chemistry protocols (GCPs) in designing or modifying a synthetic approach for the preparation of organic compounds [7a,19]. Nowadays, concerning the GCPs in the drug (or drug-like compounds) discovery process is undeniably significant and essential [20]. It is also worth mentioning that pharmaceutical

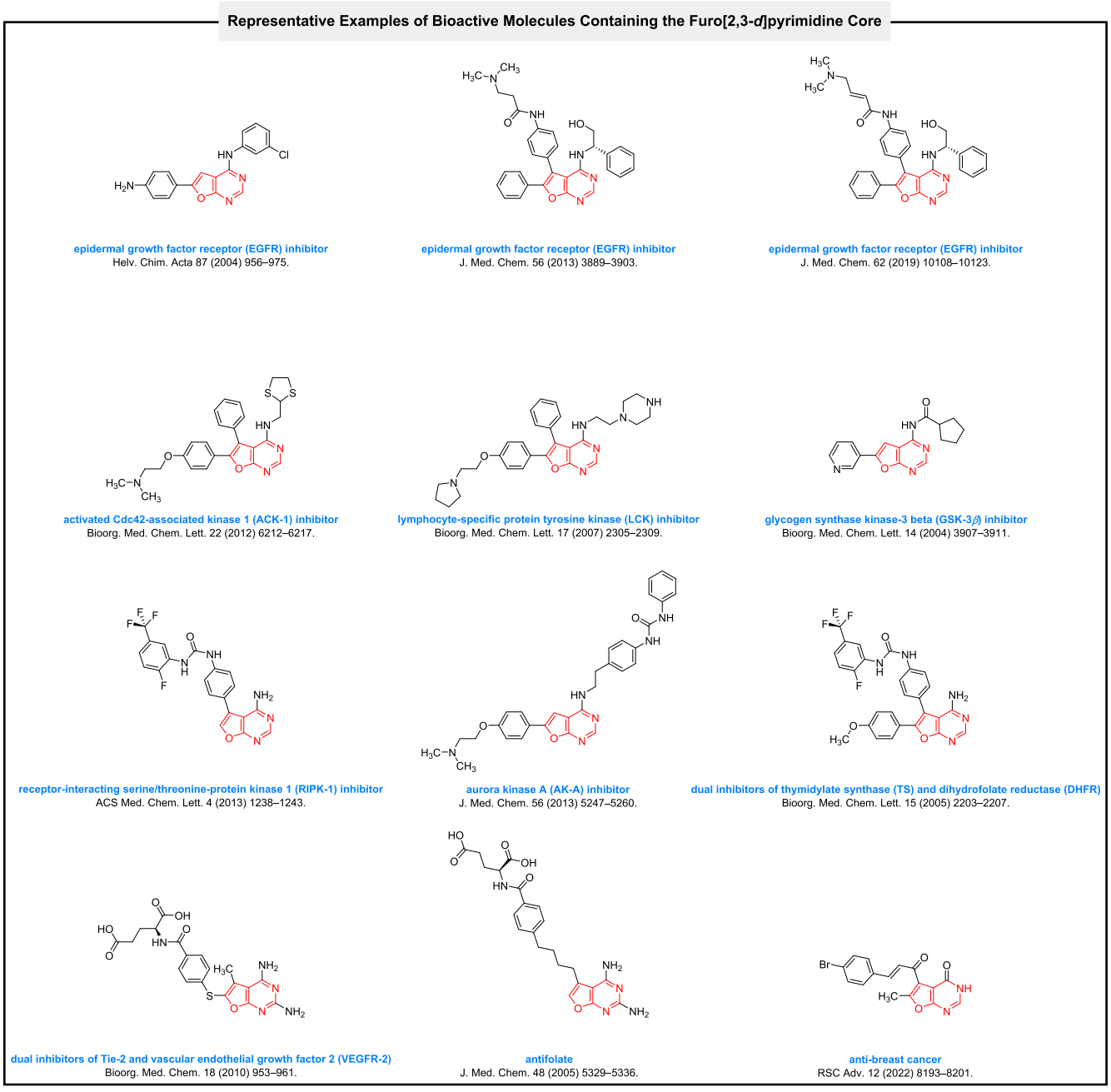

Fig. 1. Representative examples of bioactive molecules containing the furo[2,3-*d*]pyrimidine core.

manufacturing, with pioneering works, was one of the first industries to recognize the importance of the GCPs and applied all of (or most of) them as far as possible. In this regard, selecting the reaction solvent, catalyst, and procedure based on GCPs are significant. Among well-known environmentally benign chemical reaction mediums [21], water is the best because it is non-toxic, inexpensive, abundant, sustainable, and in the green chemistry solvent ranking list, holds a top and valuable place among others [22]. Furthermore, in aqueous media, it is unessential to dry co-solvents, substrates, and reagents before use, which cause saving costs and time. Catalysis is another main factor in the GCPs for the design of an environmentally benign organic reaction. Zirconium^{IV} oxychloride octahydrate ($ZrOCl_2 \bullet 8H_2O$) as an available, low-cost, easy-handling, and moisture-stable catalyst with highly coordinating ability, has attracted the attention in the organic synthetic community [23]. In the past two decades, the mentioned green catalyst has been used frequently in various organic transformations, especially heterocyclic ones, including syntheses of 4*H*-chromenes [24], pyrimido[4,5-*d*]pyrimidinones [25], dibenzo[*b*,*i*]xanthene-tetraones [26], [1,3]oxazino[5,6-*c*]quinolin-5-ones [27], 1,8-dioxo-octahydroxanthenes [28], benzopyranopyrimidines [29], 2,4,6-triarylpyridines [30], tetrahydropyrimidine [31], isobenzofuran-1(3*H*)-ones [32], 1*H*-imidazoles [33], 2-aryloxazolines [34], dihydroquinolinones [35], 3,4-dihydropyrimidin-2(1*H*)-ones [36], hexahydroquinolines [37], pyrano[2,3-*d*:6,5-*d'*]dipyrimidinones [38], pyrimido[4,5-*c*]pyridazines [39], 5-amino-1-aryl-1*H*-tetrazoles,[40] and many others. From the green chemistry point of view, one-pot multi-component reactions (MCRs) are amiable, advanced, and innovative strategies in organic synthesis [41]. Rather than the classical sequential pathway approaches, these reactions have attracted expanded attention in combinatorial, synthetic, and pharmaceutical chemistry for their distinct advantages, such as straightforward reaction design, high atom-economy, time-effectiveness, simplified work-up procedures, high overall yields of desired products, and molecular diversity. A literature survey shows that arylglyoxal monohydrate-based [42] and isocyanide-based [43] one-pot multi-component reactions have a unique place in the synthesis of the heterocyclic compounds, each independently. Therefore, the combination of mentioned starting materials in specific one-pot MCRs assuredly leads to the creation of a new avenue in novel heterocyclic scaffolds synthesis.

In continuation of our research programs on the synthesis of pharmaceutically interesting heterocyclic frameworks [44], and also due to the importance of introducing new anti-SARS-CoV-2 agents, we wish to report an environmentally benign and efficient one-pot three-component regioselective synthetic strategy for the preparation of novel 5-aroyl(or heteroaroyl)-6-(alkylamino)-1,3-dimethylfuro[2,3-*d*]pyrimidine-2,4(1*H*,3*H*)-diones (**4a–n**) through the sequential condensation of aryl(or heteroaryl)glyoxal monohydrates (**1a–g**), 1,3-dimethylbarbituric acid (**2**), and alkyl(viz. cyclohexyl or *tert*-butyl)isocyanides (**3a** or **3b**), which catalyzed by a tremendously small amount of $ZrOCl_2 \bullet 8H_2O$ (just 2 mol%), in water at 50 ℃ (Fig. 2). Besides, inhibitory activities of the newly synthesized fused heterocyclic frameworks (**4a–n**) against the active site and putative allosteric hotspots of both SARS-CoV-2 M^{Pro} and PL^{Pro} investigated using molecular docking, and the obtained results compared with various medicinal compounds, which used, introduced,

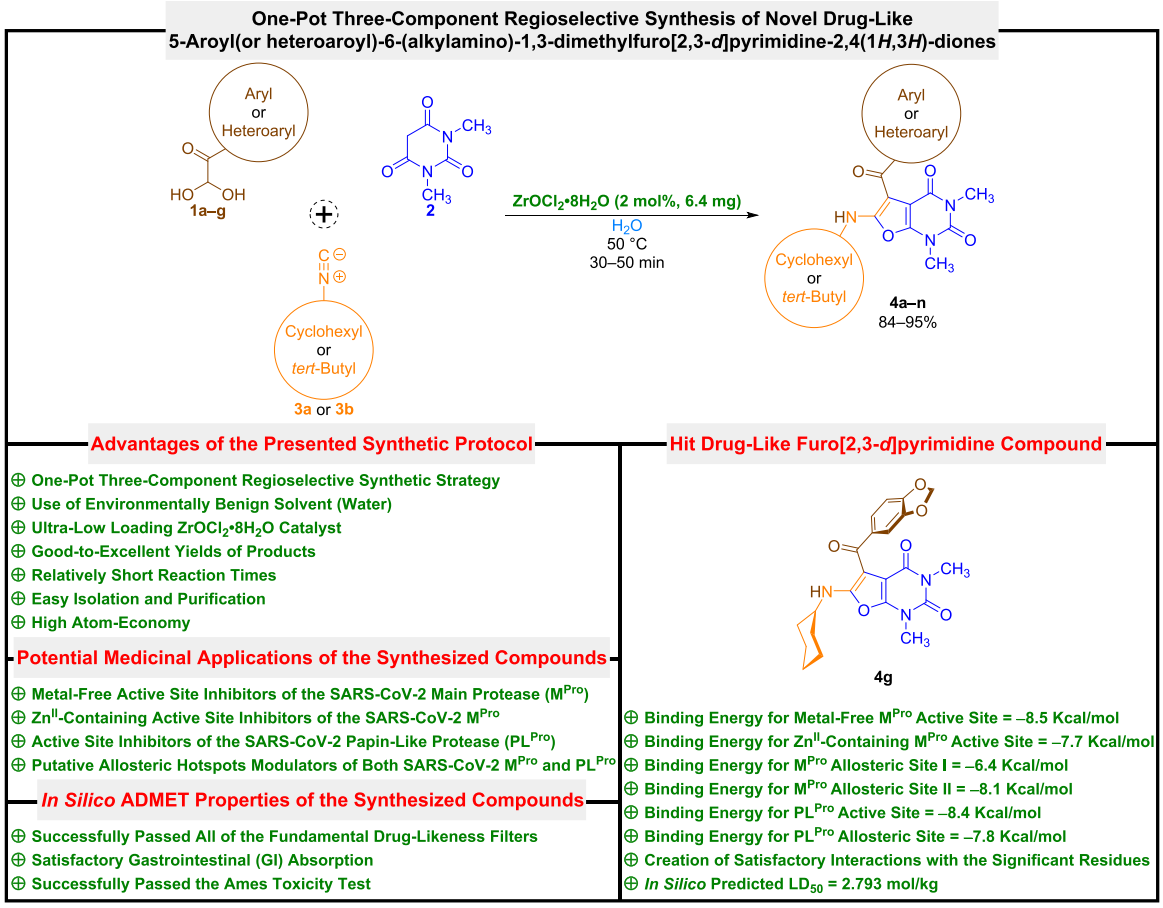

Fig. 2. Green one-pot three-component synthesis of novel drug-like furo[2,3-*d*]pyrimidines as potential active site inhibitors and putative allosteric hotspots modulators of both SARS-CoV-2 M^{Pro} and PL^{Pro}. (For interpretation of the references to colour in this figure legend, the reader is referred to the web version of this article.)

and or repurposed to fight against COVID-19 viral disease in nearly past three years. Drug-likeness properties of the mentioned furo[2,3-*d*]pyrimidines (**4a–n**) were also explored by employing *in silico* ADMET analyses. It is worthwhile to note that 5-(3,4-methylendioxybenzoyl)-6-(cyclohexylamino)-1,3-dimethylfuro[2,3-*d*]pyrimidine-2,4(1*H*,3*H*)-dione (**4g**) as hit compound is potential COVID-19 drug candidate and can subject to further *in vitro* and *in vivo* studies.

2. Results and discussion

*2.1. Synthesis, characterization, and plausible mechanism of 5-aroyl(or heteroaroyl)-6-(alkylamino)-1,3-dimethylfuro[2,3-d]pyrimidine-2,4 (1H,3H)-diones (**4a–n**)*

Initially, we commenced our studies with the optimization reaction conditions for the green one-pot regioselective synthesis of 5-benzoyl-6-(cyclohexylamino)-1,3-dimethylfuro[2,3-*d*]pyrimidine-2,4(1*H*,3*H*)-dione (**4a**) through the tandem three-component condensation of phenylglyoxal monohydrate (**1a**), 1,3-dimethylbarbituric acid (**2**), and cyclohexyl isocyanide (also known as isocyanocyclohexane) (**3a**) as a model reaction (Table 1). It is worthwhile to note that in all stages of optimization, we used water as an entirely environmentally benign reaction solvent because one of our main goals was to design a reaction based on green chemistry protocols. Under the catalyst-free conditions at room temperature, just 30% yield of the desired product (**4a**) was obtained, even after 48 h (Table 1, entry 1). Increasing reaction temperature from room temperature to 50 ℃ and Reflux caused preparation **4a** in 56% and 43%, respectively, after 24 h (Table 1, entries 2 and 3). The gained poor results led us to use a catalyst to achieve better and more efficient outcomes. To this purpose, we used 1,5-diazabicyclo [4.3.0]non-5-ene (DBN), 1,8-diazabicyclo[5.4.0]undec-7-ene (DBU), and 1,4-diazabicyclo[2.2.2]octane (DABCO) as base organocatalysts, and also zirconium^{IV} oxychloride octahydrate ($ZrOCl_2{\bullet}8H_2O$) as a green metallic catalyst. When the one-pot three-component reaction was carried out in 2 mol% presence of the mentioned easily accessible catalysts, we observed that the catalytic performance of $ZrOCl_2{\bullet}8H_2O$ is better than others at 50 ℃ (Table 1, entry 7). Further investigations showed that the decreasing and even increasing amount of $ZrOCl_2{\bullet}8H_2O$ not only did the conditions of the one-pot reaction not improve, but it made the situation worse (Table 1, entries 8 and 9). Once we had the optimized reaction conditions in hand (Table 1, entry 7), we evaluated the scope and limitations of the mentioned green one-pot three-component regioselective synthetic protocol, as shown in Fig. 3. The one-pot three-component reaction tolerated several aryl(or heteroaryl)glyoxal monohydrates (**1a–g**) and alkyl(cyclohexyl or *tert*-butyl)isocyanides (**3a** or **3b**), affording the corresponding 5-aroyl(or heteroaroyl)-6-(alkylamino)-1,3-dimethylfuro[2,3-*d*]pyrimidine-2,4(1*H*,3*H*)-diones (**4a–n**) with good-to-excellent yields. Notably, the yields of the desired furo [2,3-*d*]pyrimidine heterocyclic products containing cyclohexyl isocyanide (**3a**) were slightly better rather than *tert*-butyl isocyanide (also known as 2-isocyano-2-methylpropane) (**3b**), as shown in Fig. 3.

The structure of all mentioned fused heterocyclic products (**4a–n**) was confirmed by Fourier transform infrared spectroscopy (FT-IR), ^{1}H and ^{13}C nuclear magnetic resonance (^{1}H NMR and ^{13}C NMR), and carbon–hydrogen–nitrogen (CHN) analyses. In this regard, the ^{1}H NMR spectrum of **4a**, as a simple instance (Figure S1, section **A**), revealed a doublet peak at δ_H 8.61 ppm ($J = 8.3$ Hz) for the —NH— proton. The five aromatic protons of the phenyl ring system appeared at δ_H 7.62 ppm (d, $J = 6.9$ Hz, 2H, Ph—H), 7.51 ppm (t, $J = 7.3$ Hz, 1H, Ph—H), and 7.40 ppm (t, $J = 7.5$ Hz, 2H, Ph—H). The proton of the N—$CH_{cyclohexyl}$ has also appeared as a multiplet peak at δ_H 3.81–3.70 ppm. The two sharp singlet peaks at δ_H 3.58 ppm and 3.29 ppm are related to the two methyl groups of the pyrimidine ring (N—CH_3). Also, the four multiplet peaks at δ_H 2.11–1.41 ppm showed ten hydrogens related to the five methylene (—CH_2—) groups of the cyclohexyl homocyclic ring system. On the other hand, the ^{1}H-decoupled ^{13}C NMR (^{13}C{^{1}H} NMR) spectrum of **4a** (Figure S1, section **B**) showed seventeen peaks in agreement with the represented structure. In this regard, the peak of the benzoyl carbonyl group is revealed at δ_C 189.20 ppm, and the peaks of the two amide carbonyl groups of the pyrimidine ring are exposed at δ_C 161.09 ppm and 156.56 ppm. It is worth noting that the characteristic peaks at δ_C 149.97 ppm and 148.90 ppm are related to the two carbon atoms of the furan ring, which are nearby the oxygen heteroatom (namely C_6 and C_{7a}). Also, the other two carbon atoms of the mentioned furan ring, which are far from the furan's oxygen heteroatom (namely C_5 and C_{4a}), are visible at δ_C 94.40 ppm and 92.55 ppm. The carbons of the phenyl ring appeared at δ_C 140.39 ppm, 131.15 ppm, 128.46 ppm, and 127.33 ppm. Furthermore, the ^{13}C{^{1}H} NMR spectrum of **4a** represented one peak at δ_C 51.91 ppm for the methine group of the cyclohexyl moiety (N—$CH_{cyclohexyl}$), and two distinct peaks at δ_C 33.43 ppm and 29.69 ppm

Table 1
Optimization reaction conditions for the one-pot three-component synthesis of **4a**.

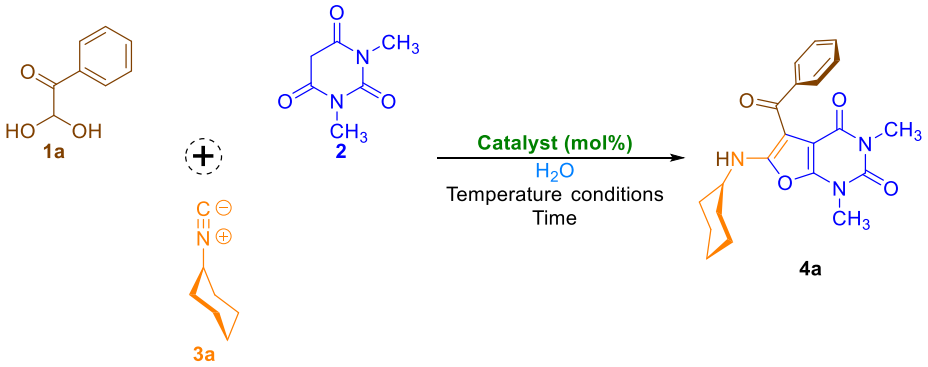

Entry	Catalyst (mol%)	Temperature conditions	Time (h or min)	Yield (%)
1	Catalyst-free	Room temperature	48 h	30
2	Catalyst-free	50 ℃	24 h	56
3	Catalyst-free	Reflux	24 h	43
4	DBN (2 mol%)	50 ℃	1 h	71
5	DBU (2 mol%)	50 ℃	1 h	75
6	DABCO (2 mol%)	50 ℃	1 h	80
7	$ZrOCl_2{\bullet}8H_2O$ (2 mol%)	50 ℃	45 min	90
8	$ZrOCl_2{\bullet}8H_2O$ (1 mol%)	50 ℃	70 min	81
9	$ZrOCl_2{\bullet}8H_2O$ (10 mol%)	50 ℃	45 min	82

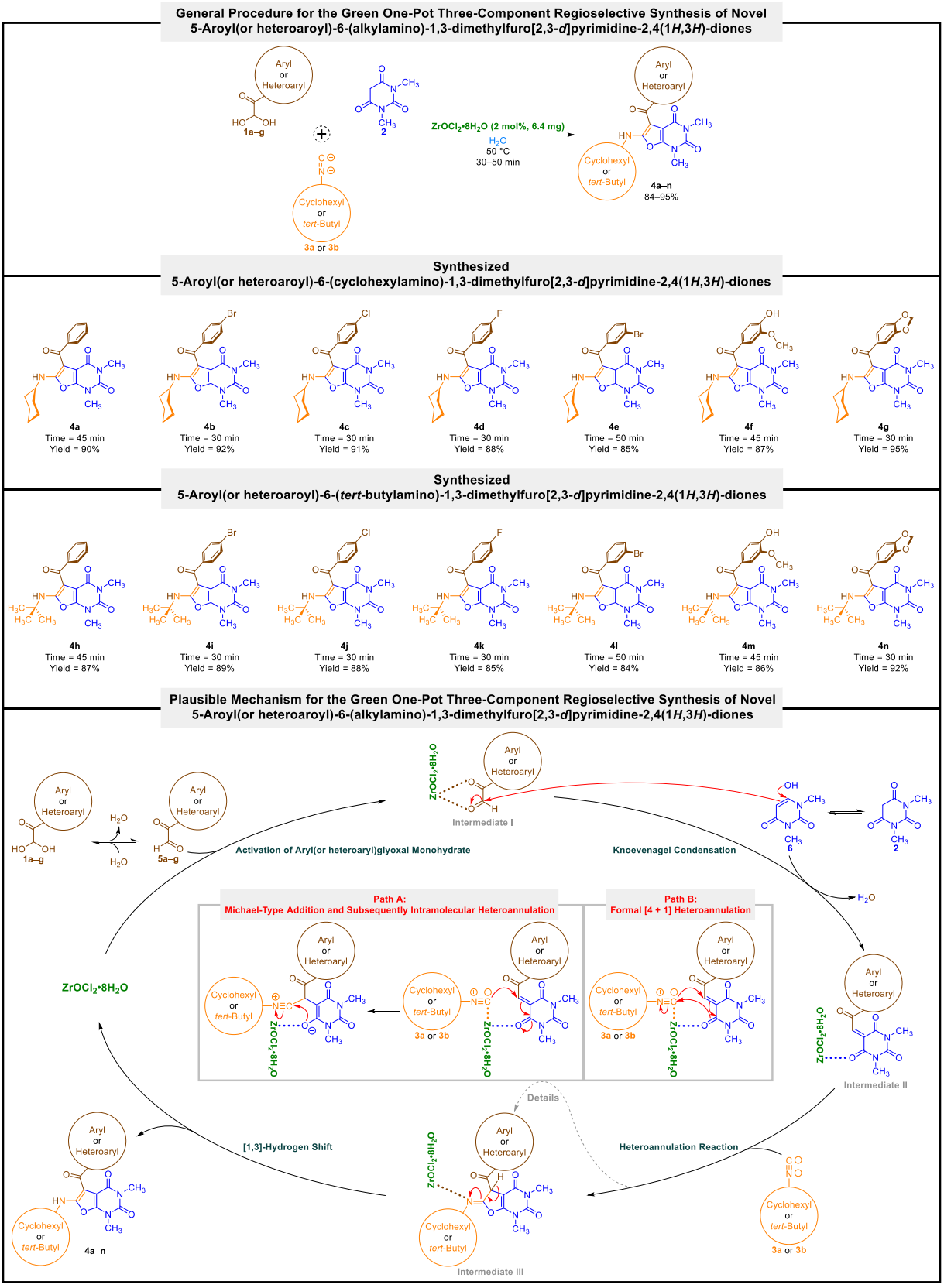

Fig. 3. Green one-pot three-component regioselective synthesis of 5-aroyl(or heteroaroyl)-6-(alkylamino)-1,3-dimethylfuro[2,3-*d*]pyrimidine-2,4(1*H*,3*H*)-diones catalyzed by $ZrOCl_2 \bullet 8H_2O$. (For interpretation of the references to colour in this figure legend, the reader is referred to the web version of this article.)

for the two N—CH_3 groups of the pyrimidine ring, and also three peaks at δ_C 28.69 ppm, 25.24 ppm, and 24.34 ppm for the cyclohexyl ring methylene groups (—CH_2—).

A plausible mechanism for this valuable green one-pot three-component regioselective transformation using $ZrOCl_2 \bullet 8H_2O$ catalyst in water at 50 ℃ is also depicted in Fig. 3. In the first step, selected aryl(or heteroaryl)glyoxal monohydrate (**1a–g**) was activated by $ZrOCl_2 \bullet 8H_2O$ and gave intermediate **I**. In the second step, a regioselective Knoevenagel condensation reaction between enol form (**6**) of 1,3-dimethylbarbituric acid (**2**) with the formyl group of the activated aryl(or heteroaryl)glyoxal (**I**) led to the formation of 1,3-dimethyl-5-(2-oxo-2-aryl(or heteroaryl)ethylidene)pyrimidine-2,4,6(1*H*,3*H*,5*H*)-trione (intermediate **II**) along with the elimination of one water molecule. In the third step, a heteroannulation reaction between the activated intermediate **II** and related alkyl(cyclohexyl or *tert*-butyl)isocyanide (**3a** or **3b**) caused the formation of (*Z*)-5-aroyl(or heteroaroyl)-6-(alkylimino)-1,3-dimethyl-5,6-dihydrofuro[2,3-*d*]pyrimidine-2,4(1*H*,3*H*)-dione (intermediate **III**). It is worth noting that the mentioned step probably proceeds from a simple Michael-type addition and subsequently intramolecular heteroannulation reaction (**path A**) and or through a formal [4 + 1] heteroannulation process (**path B**). Finally, the spurred iminolactone (intermediate **III**) generated desired furo[2,3-*d*]pyrimidine product (**4a–n**) by a [1,3]-hydrogen transfer.

2.2. Molecular docking studies

To explore the protein–ligand interactions between the newly synthesized 5-aroyl(or heteroaroyl)-6-(alkylamino)-1,3-dimethylfuro[2,3-*d*]pyrimidine-2,4(1*H*,3*H*)-diones (**4a–n**) and various pockets of the SARS-CoV-2 M^{Pro} and PL^{Pro}, *in silico* molecular docking studies performed using AutoDock Vina as an open-source program for doing molecular docking along with UCSF Chimera as a graphical user interface. First of all, we carried out a molecular docking process for our synthesized furo[2,3-*d*]pyrimidines (**4a–n**) on the active site of M^{Pro}

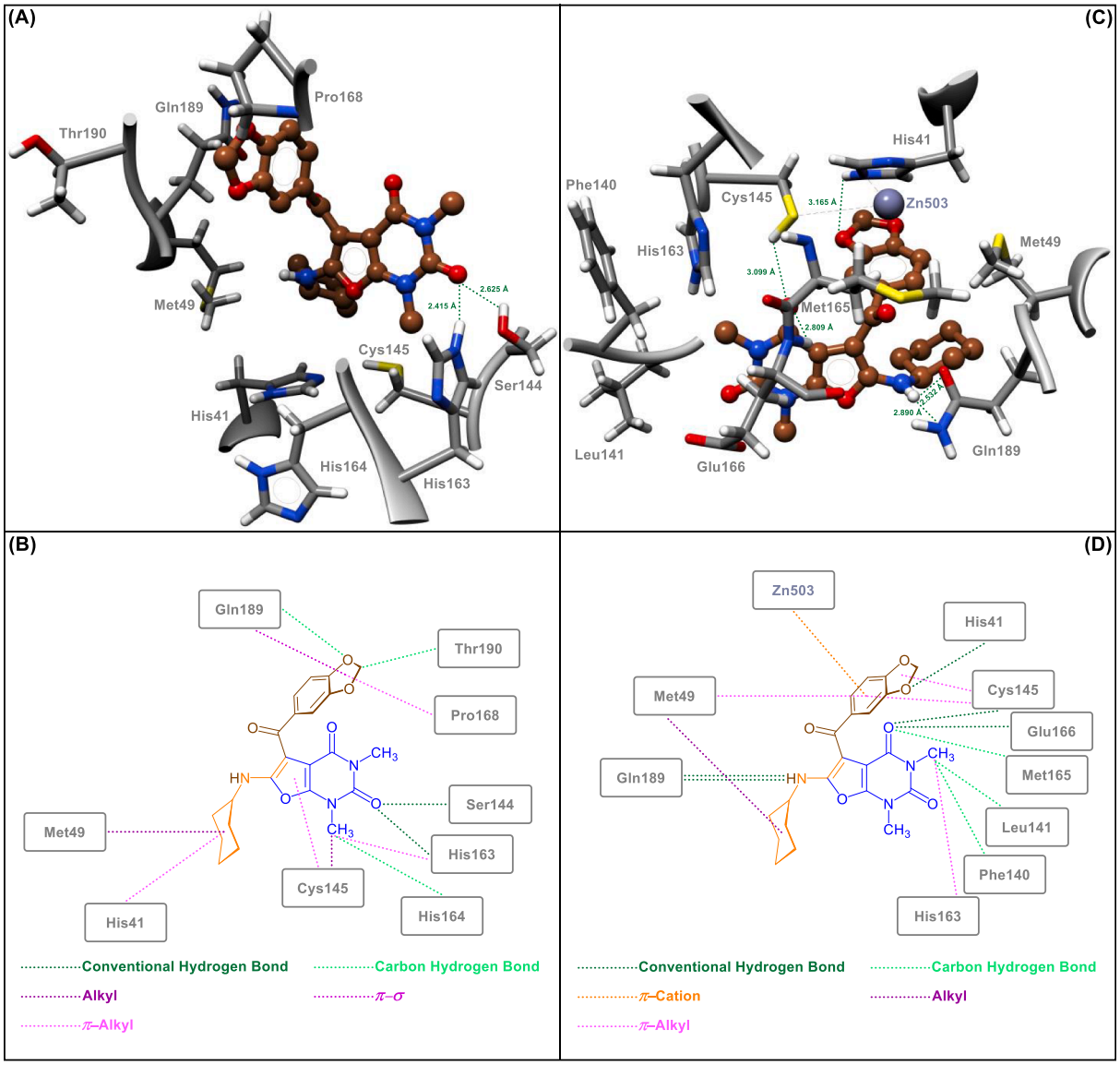

Fig. 4. Close-up views (3D and 2D) of **4g** in the metal-free active site (**A** and **B**) and Zn^{II}-containing active site (**C** and **D**) of the SARS-CoV-2 M^{Pro}, respectively.

protein (PDB ID: 7AEH). It should be noted that M^{Pro} of the SARS-CoV-2 contains a highly conserved catalytic dyad comprising amino acid residues His41 and Cys145 that are buried in the active site cavity of the mentioned protein, in which His41 acts as a general acid or base, and on the other site, Cys145 acts as a nucleophile. The obtained binding energies (also known as binding free energies, binding affinities, and or binding scores) of the molecular docking investigations were ranging from −7.2 Kcal/mol to −8.5 Kcal/mol (Table S1). From the binding energy point of view, the attained results demonstrated that 5-(3,4-methylendioxybenzoyl)-6-(cyclohexylamino)-1,3-dimethylfuro[2,3-*d*] pyrimidine-2,4(1*H*,3*H*)-dione (**4g**) with a binding energy of −8.5 Kcal/mol is slightly better than other synthesized furo[2,3-*d*]pyrimidine heterocyclic frameworks (**4a−n**). As shown in Fig. 4 (sections **A** and **B**) and Table S1, the compound **4g** was able to form two conventional hydrogen bonds with residues Ser144 (2.625 Å) and His163 (2.415 Å) of the SARS-CoV-2 M^{Pro} active site. On the other hand, **4g** has some hydrophobic interactions with His41/Cys145 catalytic dyad. In this regard, the compound **4g** exhibited *π*–alkyl interaction with His41 and revealed alkyl and *π*–alkyl interactions with Cys145. Furthermore, the mentioned fused heterocyclic compound (**4g**) interacts with residues Met49 (alkyl), His163 (*π*–alkyl), His164 (carbon hydrogen bond), Pro168 (*π*–alkyl), Gln189 (carbon hydrogen bond and *π*–*σ*), and Thr190 (carbon hydrogen bond), as shown in Fig. 4 (sections **A** and **B**) and Table S1. Interestingly, as shown in Table S1, the compound 5-(4-hydroxy-3-methoxybenzoyl)-6-(cyclohexylamino)-1,3-dimethylfuro[2,3-*d*]pyrimidine-2,4(1*H*,3*H*)-dione (**4f**), with a binding energy of −7.9 Kcal/mol, capable to creation eight hydrogen bonds with the SARS-CoV-2 M^{Pro} active site residues, especially Cys145 (2.341 Å). In 2022, Ebrahim and co-workers published a valuable and attention-grabbing paper about the temperature-dependent conformational ensemble of the SARS-CoV-2 M^{Pro} [45]. Their studies revealed that in human body temperature (310 K), the mobile zinc^{II} (Zn^{II}) ion interleaved between the His41/Cys145 catalytic dyad (Figure S2). The mentioned occurrence can inspire the scientific community to make new and different plans for designing new covalent and non-covalent SARS-CoV-2 M^{Pro} inhibitors. To this purpose, we shifted our investigations to the Zn^{II}-containing active site of the SARS-CoV-2 M^{Pro} protein (PDB ID: 7MHK). For this stage, the obtained binding energies were ranging from −6.5 Kcal/mol to −7.7 Kcal/mol (Table S2). Gratifyingly, in terms of binding energy we saw that the best heterocyclic compound was **4g** (−7.7 Kcal/mol). As shown in Fig. 4 (sections **C** and **D**) and Table S2, the compound **4g** can form five conventional hydrogen bonds with His41 (3.165 Å), Cys145 (3.099 Å), Glu166 (2.809 Å), and Gln189 (2.532 Å and 2.890 Å). In addition, we observed a *π*–cation interaction between **4g** and Zn^{II} ion (Zn503). Furthermore, the compound **4g** interacts with Met49 (alkyl and *π*–alkyl), Phe140 (carbon hydrogen bond), Leu141 (carbon hydrogen bond), Cys145 (*π*–alkyl),

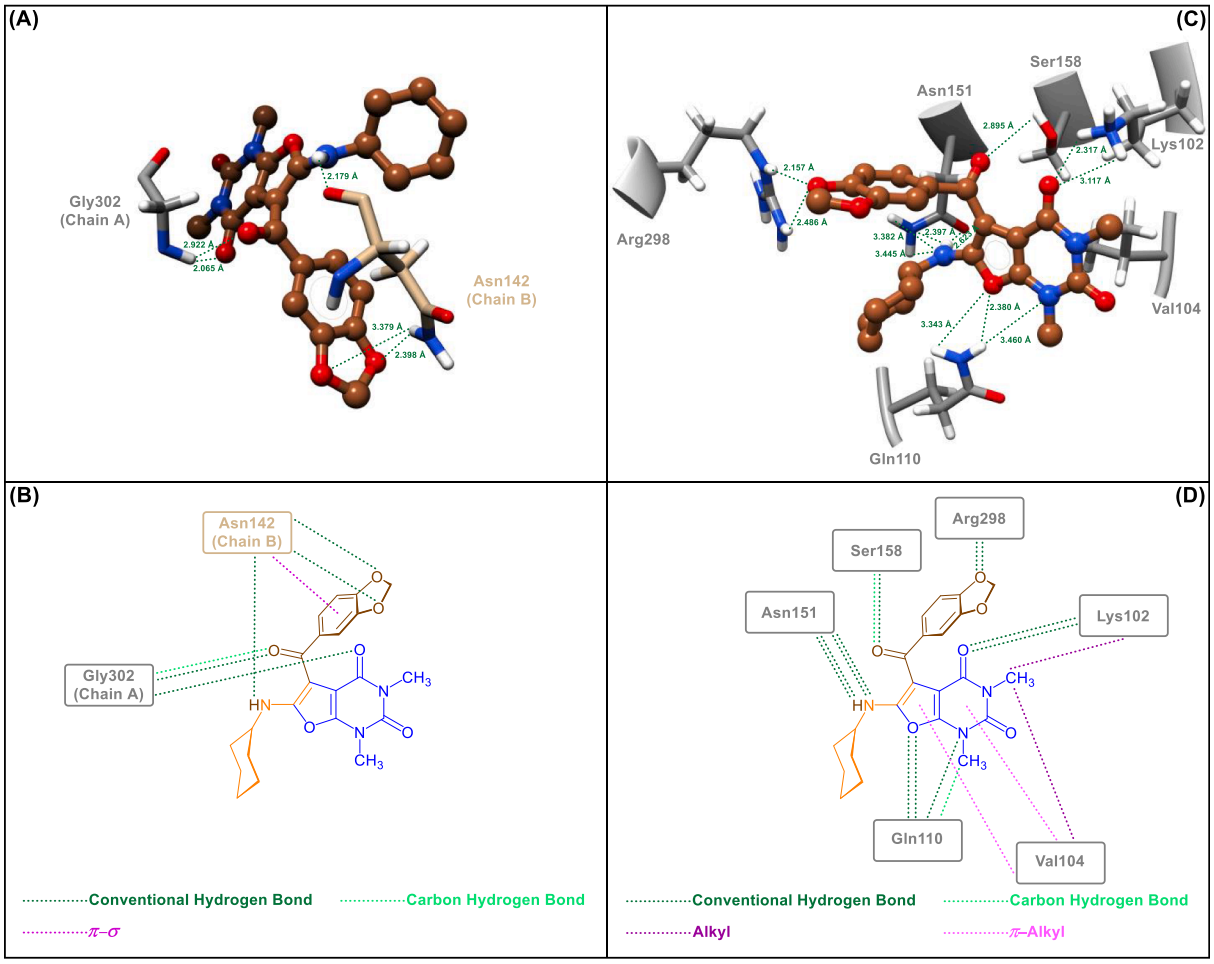

Fig. 5. Close-up views (3D and 2D) of **4g** in the allosteric site I (**A** and **B**) and allosteric site II (**C** and **D**) of the SARS-CoV-2 M^{Pro}, respectively.

His163 (π–alkyl), and Met165 (carbon hydrogen bond) (Fig. 4 (sections **C** and **D**) and Table S2). It is worth noting that, as shown in Table S2, the compound **4f**, with a binding energy of −7.5 Kcal/mol, is capable to create eleven hydrogen bonds with the SARS-CoV-2 M^{Pro} active site residues, especially three hydrogen bonds with Cys145 (2.470 Å, 2.830 Å, and 3.128 Å), and also can form a metal–acceptor interaction with Zn503.

Inhibition of allosteric hotspots is an emerging paradigm in modern pharmacology to the extent that recent years have seen an unprecedented and astonishing level of innovation in the discovery and development of allosteric drugs [46]. Because of the importance of this issue, we investigated the molecular docking process for two putative allosteric pockets of the SARS-CoV-2 M^{Pro}, including allosteric site I (known as dimerization site, which could interrupt the dimerization conformation and inactive the M^{Pro}) and allosteric site II (Known as cryptic site) [47]. The molecular docking results for the allosteric site I (PDB ID: 7VLP) showed that the binding energies of the investigations were ranging from −5.3 Kcal/mol to −6.4 Kcal/mol (Table S3), which the compound **4g** with a binding energy of −6.4 Kcal/mol is somewhat better than others, and as shown in Fig. 5 (sections **A** and **B**) and Table S3, it was able to form two conventional hydrogen bonds with residue Gly302A (2.065 Å and 2.922 Å) and three conventional hydrogen bonds with residue Asn142B (2.179 Å, 2.398 Å, and 3.379 Å). Furthermore, we observed a carbon hydrogen bond interaction with Gly302A and a π–σ hydrophobic interaction with Asn142B, as shown in Fig. 5 (sections **A** and **B**) and Table S3. On the other hand, the molecular docking outcomes for allosteric site II (PDB: 7MHK) exhibited that the binding energies were ranging from −6.6 Kcal/mol to −8.1 Kcal/mol (Table S4), which again the compound **4g** with a binding energy of −8.1 Kcal/mol is slightly better than others. As shown in Fig. 5 (sections **C** and **D**) and Table S4, **4g** can able to create twelve conventional hydrogen bonds with residues Lys102 (2.317 Å and 3.117 Å), Gln110 (2.380 Å, 3.343 Å, and 3.460 Å), Asn151 (2.397 Å, 2.623 Å, 3.382 Å, and 3.445 Å), Ser158 (2.895 Å), and Arg298 (2.157 Å and 2.486 Å). Besides, **4g** has alkyl interaction with Lys102, and alkyl and π–alkyl interactions with Val104 along with carbon hydrogen bond interactions with Gln110 and Ser158, as shown in Fig. 5 (sections **C** and **D**) and Table S4.

The SARS-CoV-2 PL^{Pro} is another essential factor for the COVID-19

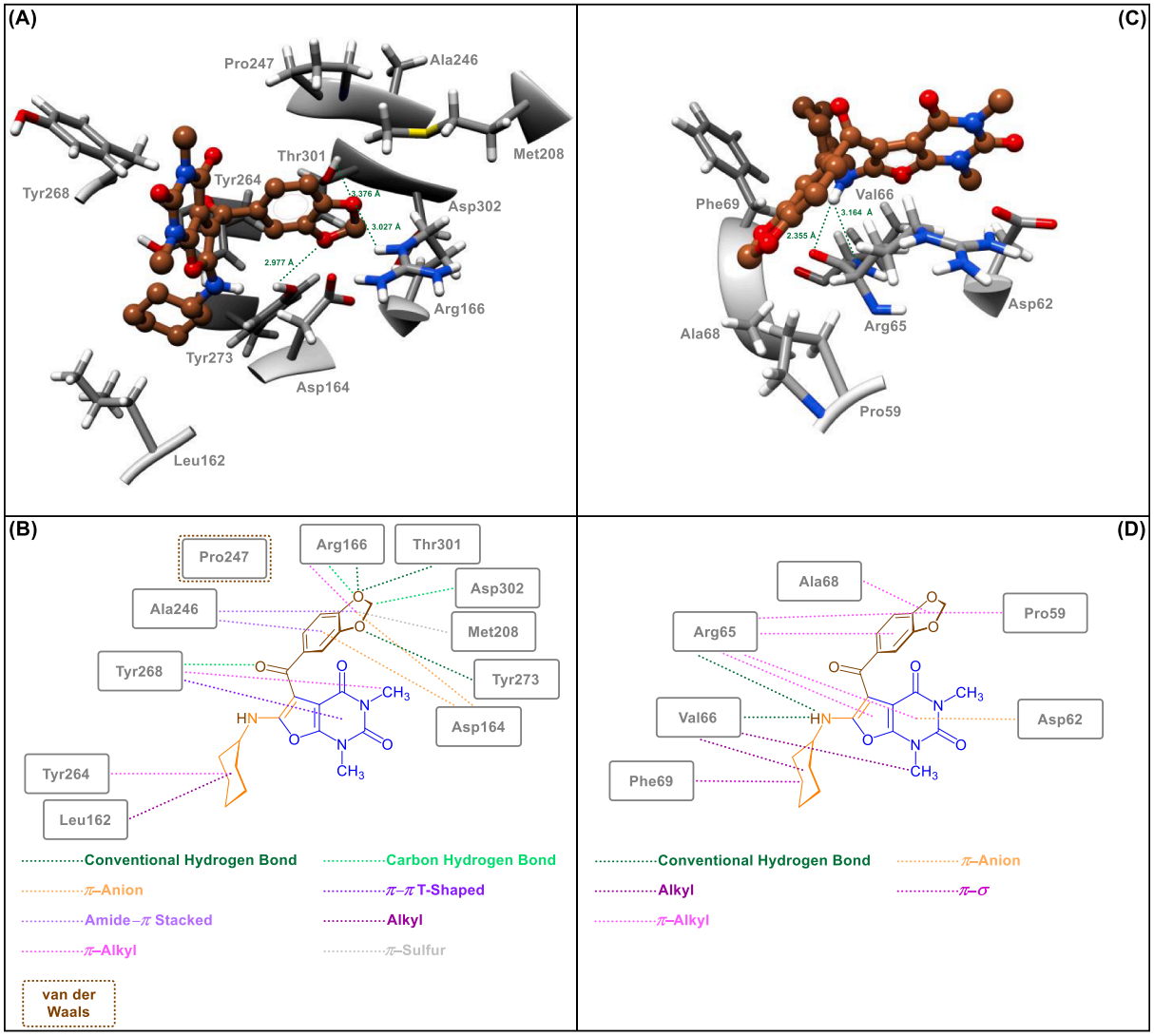

Fig. 6. Close-up views (3D and 2D) of **4g** in the active site (**A** and **B**) and allosteric site (**C** and **D**) of the SARS-CoV-2 PL^{Pro}, respectively.

proliferation cycle. The mentioned SARS-CoV-2 PL^{Pro} active site contains the catalytic triad that is formed by Cys111, His272, and Asp286. In continuation of *in silico* studies, we investigated another molecular docking process for our synthesized furo[2,3-*d*]pyrimidines (**4a–n**) on the active site of SARS-CoV-2 PL^{Pro} protein (PDB ID: 6WX4). The molecular docking investigations showed that obtained binding energies were ranging from −7.5 Kcal/mol to −8.4 Kcal/mol (Table S5). Among the mentioned furo[2,3-*d*]pyrimidines (**4a–n**), the compound **4g** with a binding energy of −8.4 Kcal/mol is again slightly better than others. As shown in Fig. 6 (sections **A** and **B**) and Table S5, this ligand (**4g**) formed three conventional hydrogen bonds with the amino acids residues Arg166 (3.027 Å), Tyr273 (2.977 Å), and Thr301 (3.376 Å). In addition, other interactions were observed (Fig. 6 (sections **A** and **B**) and Table S5) for this case, including Leu162 (alkyl), Asp164 (*π*–anion), Arg166 (carbon hydrogen bond and *π*–alkyl), Met208 (*π*–sulfur), Ala246 (amide–*π* stacked), Pro247 (van der Waals), Tyr264 (*π*–alkyl), Tyr268 (carbon hydrogen bond, *π*–*π* T-shaped, and *π*–alkyl), and Asp302 (carbon hydrogen bond). Remarkably, the SARS-CoV-2 PL^{Pro} (PDB ID: 6WX4) allosteric [48] inhibitory properties of our synthesized heterocyclic compounds were also investigated. The binding energies for this case were from −5.8 Kcal/mol to −7.8 Kcal/mol (Table S6). The compound **4g**, which is better than others in terms of binding energy (−7.8 Kcal/mol), can able to form two conventional hydrogen bonds with residues Arg65 (2.355 Å) and Val66 (3.164 Å), as shown in Fig. 6 (sections **C** and **D**) and Table S6. On the other hand, **4g** have hydrophobic interactions with residues Pro59 (*π*–alkyl), Arg65 (*π*–alkyl), Val66 (alkyl), Ala68 (*π*–alkyl), and Phe69 (*π*–*σ*), along with an electrostatic interaction with residue Asp62 (*π*–anion) (Fig. 6 (sections **C** and **D**) and Table S6).

2.3. *In silico* ADMET prediction

Most of the designed and prepared chemical compounds for medicinal purposes fail and flop in the drug development process due to their poor pharmacokinetics and toxicity problems, which is an undeniable fact worth pondering. Such drawbacks that arise during drug development should be addressed at the early stage in the pipeline of this process to prevent the loss of material and intellectual capital and to achieve the desired goal in a shorter period of time and with low costs. *In silico* ADMET (absorption, distribution, metabolism, excretion, and toxicity) prediction is a significant analysis to rolling out undesired effects of a proposed drug candidate at the initial step of the drug discovery process [49]. In this regard, *in silico* ADME analysis of the prepared 5-aroyl(or heteroaroyl)-6-(alkylamino)-1,3-dimethylfuro[2,3-*d*]pyrimidine-2,4(1*H*,3*H*)-diones (**4a–n**) investigated using free web tool SwissADME, from Swiss Institute of Bioinformatics (http://www.swissadme.ch) [50]. The data related to physicochemical properties and lipophilicity (Table S7), water solubility (Table S8), pharmacokinetics (Table S9), and drug-likeness and medicinal chemistry (Table S10) of the synthesized heterocyclic compounds (**4a–n**) have been collected in Supporting Information (SI). Interestingly, the obtained results demonstrated the mentioned furo[2,3-*d*]pyrimidines (**4a–n**) generally possess drug-like behavior because they could successfully be passed fundamental drug-likeness filters, including Lipinski (Pfizer), Ghose (Amgen), Veber (GSK), Egan (Pharmacia), and Muegge (Bayer). Also, the Abbot bioavailability score [51] value for all synthesized compounds (**4a–n**) was 0.55 (55%), which indicates the probability of their bioavailability, and it is based on the total charge of compound, topological polar surface area (TPSA), and violation of Lipinski filter. Furthermore, pan assay interference structures (PAINS) and Brenk filters are applied to provide information concerning potentially problematic fragments (putatively toxic, metabolically unstable, or possessing properties responsible for poor pharmacokinetics). Gratifyingly, our heterocyclic frameworks (**4a–n**) have no alert for PAINS and Brenk. On the other hand, the BOILED-Egg plot between WLOGP and TPSA was used to predict gastrointestinal absorption and brain penetration of the furo[2,3-*d*]pyrimidines (**4a–n**). As can be seen from the BOILED-Egg plot (Fig. 7), all of the mentioned one-pot synthesized compounds (**4a–n**) show satisfactory gastrointestinal (GI) absorption and have no blood–brain barrier (BBB) permeability, and the red dots as P-glycoprotein non-substrates (PGP−) demonstrate predictions that our fused heterocyclic compounds (**4a–n**) cannot be effluxes from the central

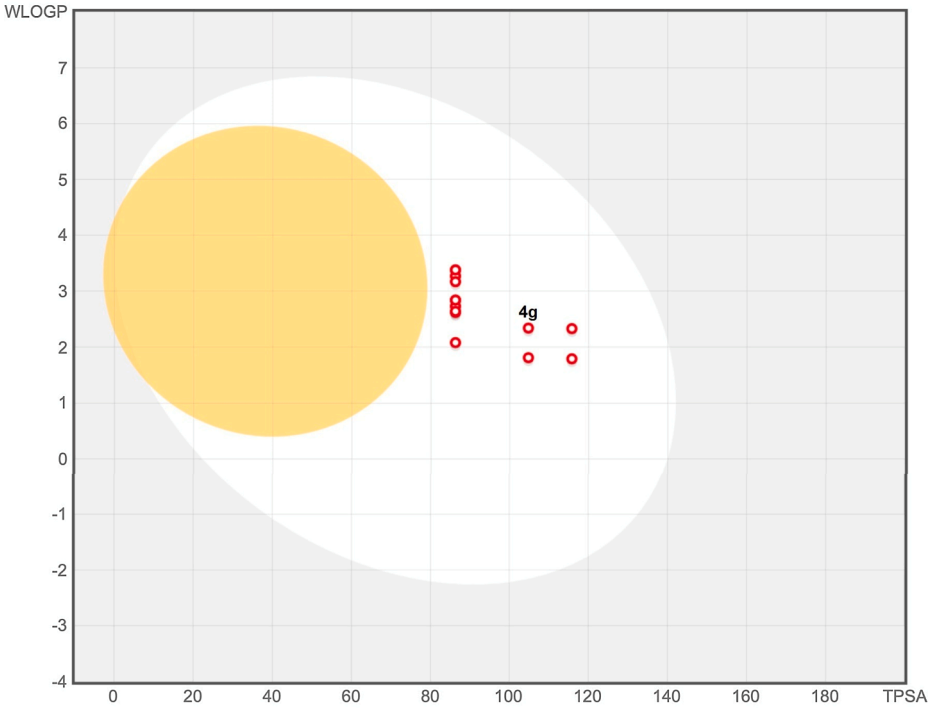

Fig. 7. BOILED-Egg plot of 5-aroyl(or heteroaroyl)-6-(alkylamino)-1,3-dimethylfuro[2,3-*d*]pyrimidine-2,4(1*H*,3*H*)-diones.

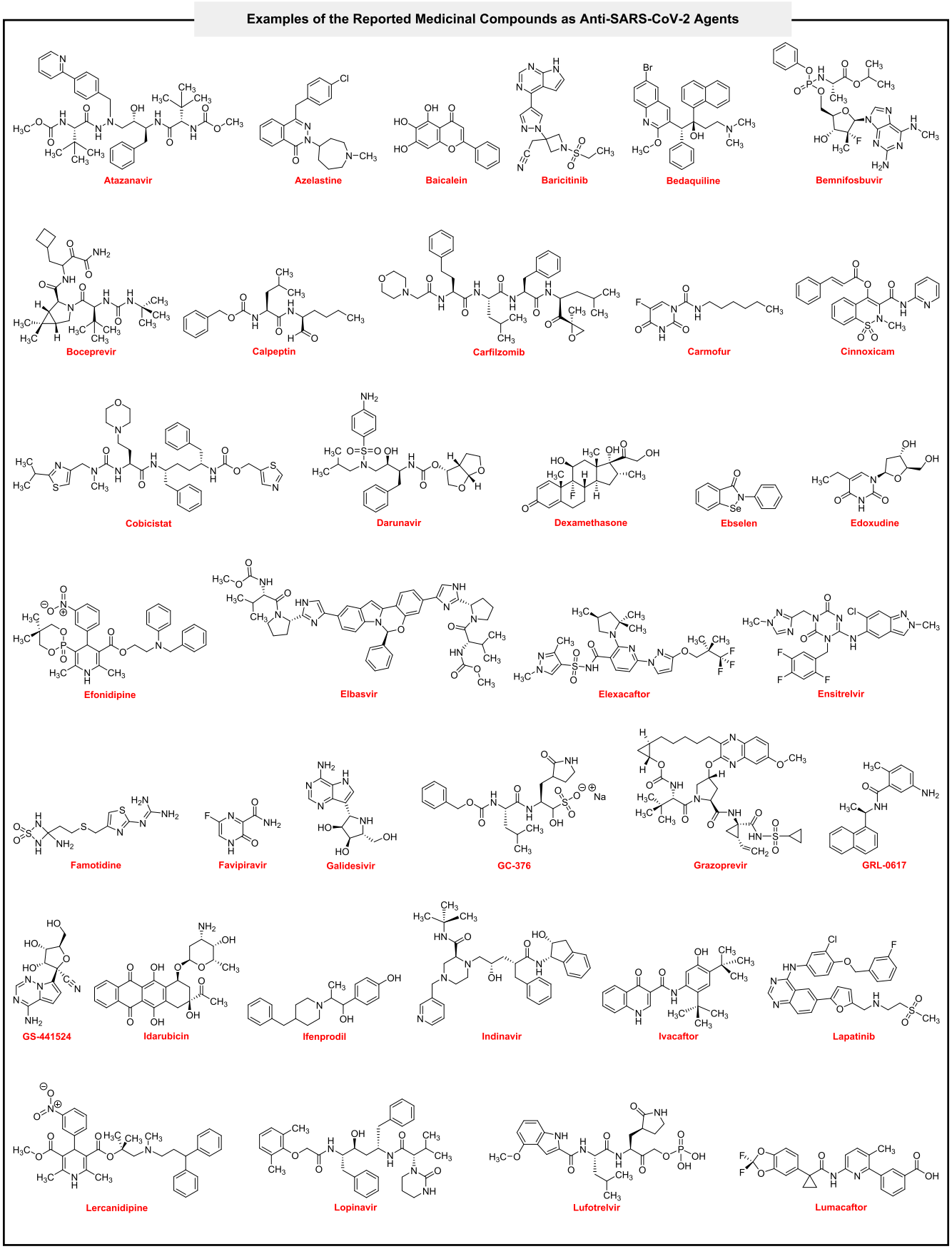

Fig. 8. Examples of the reported medicinal compounds as anti-SARS-CoV-2 agents.

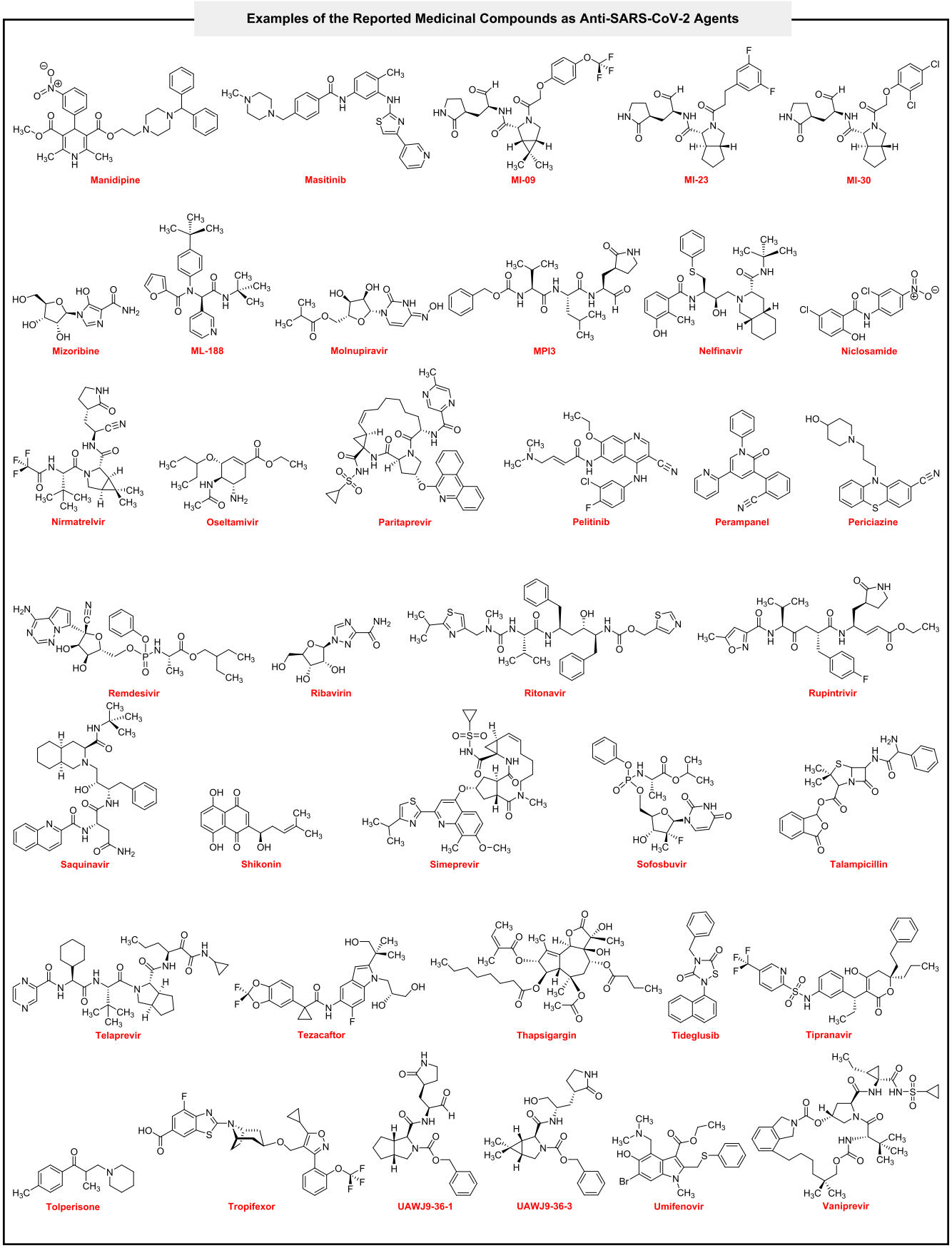

Fig. 8. (*continued*).

Table 2
Comparative molecular docking studies between **4g** and reported medicinal compounds as anti-SARS-CoV-2 agents.

Entry	Compound name	Binding energy (Kcal/mol)					
		Main protease (M^{Pro})				Papain-like protease (PL^{Pro})	
		Metal-free active site (PDB ID: 7AEH)	Zn^{II}-Containing active site (PDB ID: 7MHK)	Allosteric site I (PDB ID: 7VLP)	Allosteric site II (PDB ID: 7MHK)	Active site (PDB ID: 6WX4)	Allosteric site (PDB ID: 6WX4)
1	4g	−8.5	−7.7	−6.4	−8.1	−8.4	−7.8
2	Atazanavir	−7.1	−6.9	−5.5	−7.3	−6.4	−6.6
3	Azelastine	−7.5	−7.2	−6.1	−7.7	−7	−7.1
4	Baicalein	−7.3	−7.1	−6.3	−7.3	−7	−7.1
5	Baricitinib	−7.6	−7.4	−5.5	−7.3	−7.3	−6
6	Bedaquiline	−7.3	−7.6	−5.4	−7.4	−7.2	−7.5
7	Bemnifosbuvir	−7.5	−7.2	−5.8	−7.4	−7.1	−6.4
8	Boceprevir	−7.1	−7.1	−5.5	−7.2	−7.2	−5.7
9	Calpeptin	−6.1	−6.3	−4.8	−6.5	−5.8	−5.5
10	Carfilzomib	−6.5	−7	−6.2	−6.3	−6.3	−5.8
11	Carmofur	−6.2	−6.2	−4.9	−6.4	−6.4	−5.7
12	Cinnoxicam	−7.9	−7.8	−6.5	−8.4	−7.2	−6.7
13	Cobicistat	−6.2	−7.3	−5.9	−7.4	−7.3	−5.8
14	Darunavir	−7.6	−7	−5.8	−7.9	−7.1	−6.1
15	Dexamethasone	−7.8	−7.5	−5.4	−7.4	−7.6	−5.8
16	Ebselen	−6.2	−6.7	−5.3	−6.5	−6.1	−6.1
17	Edoxudine	−6.4	−6.4	−5.2	−6	−6.1	−5.6
18	Efonidipine	−7.3	−8.5	−6.1	−8.6	−7.8	−6.5
19	Elbasvir	−8.7	−7.5	−6.3	−8.7	−7.9	−7
20	Elexacaftor	−7.8	−7.8	−6.5	−8.7	−7.6	−6.7
21	Ensitrelvir	−9.9	−8.2	−6.6	−8.6	−7.8	−7.2
22	Famotidine	−6.2	−6.1	−4.8	−5.3	−6.8	−5
23	Favipiravir	−5.7	−5.5	−5.3	−5.5	−5.8	−5.1
24	Galidesivir	−6.6	−6.2	−6.1	−6	−6.5	−5.8
25	GC-376	−6.9	−7.5	−5.6	−7.8	−7.2	−6
26	Grazoprevir	−7.4	−7.2	−6.4	−7.8	−6.6	−6
27	GRL-0617	−7	−7.1	−6.5	−7.7	−7.7	−6.9
28	GS-441524	−6.6	−6.7	−5.1	−6.5	−6.4	−6
29	Idarubicin	−8.5	−7.4	−6.2	−7.8	−7.3	−6.8
30	Ifenprodil	−7.6	−6.9	−7	−7.2	−7	−6.6
31	Indinavir	−7.6	−7.3	−6.6	−7.7	−7.6	−7
32	Ivacaftor	−7.2	−7	−5.9	−8.4	−7.1	−6.6
33	Lapatinib	−8.4	−7.9	−7	−8.1	−7.8	−7.4
34	Lercanidipine	−7.9	−7.7	−5.1	−7.7	−7.5	−6.4
35	Lopinavir	−7.3	−7.3	−5.8	−7.1	−7.3	−6.4
36	Lufotrelvir	−7.6	−7.4	−5.6	−7.6	−7.8	−5.7
37	Lumacaftor	−8.9	−9.1	−7.9	−9.3	−8.9	−8.1
38	Manidipine	−8.3	−7.1	−5.4	−8.3	−7.9	−6.8
39	Masitinib	−7.9	−8.2	−6.6	−9.3	−8.1	−7.5
40	MI-09	−8.3	−7.8	−5.8	−8.2	−8.5	−7.3
41	MI-23	−8.2	−8.3	−6.4	−8.1	−7.4	−6.8
42	MI-30	−8.1	−8	−6.4	−8.1	−7.9	−6.7
43	Mizoribine	−6.7	−6.7	−4.5	−6.4	−6	−5.6
44	ML-188	−7.3	−7	−5.6	−6.9	−7.1	−5.5
45	Molnupiravir	−7.3	−7	−5.7	−7	−7.4	−5.9
46	MPI3	−6.7	−7.1	−4.5	−6.7	−7.3	−5.4
47	Nelfinavir	−8.2	−7.2	−6.3	−8.1	−6.8	−6.4
48	Niclosamide	−7.3	−7.1	−5.4	−7	−7	−6.4
49	Nirmatrelvir	−8	−7.6	−5.8	−7	−8.2	−6.2
50	Oseltamivir	−5.9	−5.8	−4.2	−5.8	−6.3	−5.2
51	Paritaprevir	−7.7	−7.9	−7.6	−7.8	−8	−8.3
52	Pelitinib	−7.9	−7.3	−6.1	−7.7	−7.2	−6.6
53	Perampanel	−8.1	−7.5	−5.5	−7.6	−8	−7.3
54	Periciazine	−7.7	−7.8	−5.7	−6.8	−7.4	−6.4
55	Remdesivir	−7.9	−7.3	−5.1	−6.7	−7.3	−5.7
56	Ribavirin	−6.4	−6.3	−5.4	−6.3	−6.5	−5.3
57	Ritonavir	−6.9	−6.7	−6	−7.9	−6.4	−6.1
58	Rupintrivir	−7.6	−7.3	−5.6	−6.9	−7	−6
59	Saquinavir	−7.8	−7.9	−6.5	−9.9	−7.9	−7.1
60	Shikonin	−7.3	−6.8	−5.8	−7.2	−6.9	−7.6
61	Simeprevir	−8	−7.9	−6.8	−9.5	−7.6	−7.8
62	Sofosbuvir	−7.6	−7.5	−5.6	−7	−7.3	−6.4
63	Talampicillin	−8.4	−8.1	−6.8	−8.2	−8.3	−7.1
64	Telaprevir	−7.8	−7.1	−6	−7.8	−7	−5.7
65	Tezacaftor	−7.7	−7.6	−6.7	−8.5	−7.4	−6.9
66	Thapsigargin	−6.1	−5.9	−4.6	−6.6	−6	−4.3
67	Tideglusib	−7.1	−7.4	−6.3	−7.7	−7.6	−7.3
68	Tipranavir	−7.8	−6.6	−6.7	−8.1	−7.8	−7.5
69	Tolperisone	−5.8	−6.1	−5.2	−6.7	−6.3	−6.1
70	Tropifexor	−8.1	−8.6	−6.3	−8.6	−8.6	−7.1

(*continued on next page*)

Table 2 (*continued*)

Entry	Compound name	Binding energy (Kcal/mol)					
		Main protease (M^{Pro})				Papain-like protease (PL^{Pro})	
		Metal-free active site (PDB ID: 7AEH)	Zn^{II}-Containing active site (PDB ID: 7MHK)	Allosteric site I (PDB ID: 7VLP)	Allosteric site II (PDB ID: 7MHK)	Active site (PDB ID: 6WX4)	Allosteric site (PDB ID: 6WX4)
71	UAWJ9-36-1	−7.6	−7.9	−5	−7.3	−6.5	−6
72	UAWJ9-36-3	−7.5	−7.7	−5.9	−7.5	−7.1	−6.3
73	Umifenovir	−6.2	−6.5	−4.5	−6	−6.4	−5.5
74	Vaniprevir	−8.3	−8.4	−7.3	−7	−7.1	−6

nervous system (CNS) by PGP. Overall, from the related BOILED-Egg plot data, especially from the positions of the red dots, we can conclude that the BBB penetration property and PGP effect for our compounds are negative, and the GI absorption property is positive. Besides, the *in silico* toxicity evaluation was carried out using an online server, pkCSM (https://biosig.lab.uq.edu.au/pkcsm/prediction) [52]. As shown in Table S11, the *in silico* Ames toxicity test investigation shows that all the newly synthesized fused heterocyclic frameworks (**4a–n**) successfully passed the mentioned imperative test and predicted them as non-mutagenic compounds. Also, LD_{50} (oral rat acute toxicity) amounts for these heterocyclic structures (**4a–n**) were from 2.37 mol/kg to 2.793 mol/kg, which highest one related to **4g** (Table S11).

2.4. Comparative study

To demonstrate the 5-aroyl(or heteroaroyl)-6-(alkylamino)-1,3-dimethylfuro[2,3-*d*]pyrimidine-2,4(1*H*,3*H*)-diones (**4a–n**) value and power in fighting against COVID-19 disease, we compared hit one (**4g**) with seventy-three medicinal compounds (Fig. 8) that used, repurposed, investigated, and introduced against SARS-CoV-2 in closely three past years. From the binding energy point of view, the mentioned comparison revealed that **4g** could have a unique place in this viral war. As shown in Table 2, binding energies of the medicinal compounds from the SARS-CoV-2 M^{Pro} metal-free active site (PDB ID: 7AEH) showed that only three of them (viz. Elbasvir, Ensitrelvir, and Lumacaftor) are better than **4g**, and one of them, namely Idarubicin, has equal binding energy with **4g**. Also, the molecular docking results of **4g** from the M^{Pro} Zn^{II}-containing active site (PDB ID: 7MHK), the allosteric site I (PDB ID: 7VLP), and the allosteric site II (PDB ID: 7MHK) of the SARS-CoV-2 were satisfied and acceptable rather than others. It should be noted that Ensitrelvir (known as S-217622), which is a better inhibitor than **4g** in both SARS-CoV-2 M^{Pro} metal-free and Zn^{II}-containing active sites and allosteric sites (Table 2, entry 21), was reported in 2022 as the first oral non-covalent and non-peptidic SARS-CoV-2 M^{Pro} inhibitor clinical candidate with IC_{50} value of 13 nM and have EC_{50} values for wild type (WT) and other strains of SARS-CoV-2 including alpha, betta, gamma, delta, and omicron equal 0.37 μM, 0.33 μM, 0.40 μM, 0.50 μM, 0.41 μM, and 0.29 μM, respectively [53]. Furthermore, a comparison between entries 1, 49, and 57 of Table 2 revealed that **4g** has more suitable binding energy than both Nirmatrelvir and Ritonavir as two parts of the oral Pfizer's Paxlovid SARS-CoV-2 M^{Pro} inhibitor drug for COVID-19 [54]. As shown in Table 2 (entries 1 and 44), the compound **4g** is also better SARS-CoV-2 M^{Pro} inhibitor than ML-188 (with a IC_{50} of 2.5 ± 0.3 μM) as a non-covalent M^{Pro} inhibitor [55]. In the SARS-CoV-2 PL^{Pro} active site (PDB ID: 6WX4), Lumacaftor, MI-09, and Tropifexor (Table 2, entries 37, 40, and 70) showed slightly better binding energy than **4g**, and also in the SARS-CoV-2 PL^{Pro} allosteric site (PDB ID: 6WX4), Lumacaftor and Paritaprevir (Table 2, entries 37 and 51) were somewhat better than **4g**, and Simeprevir (Table 2, entry 61) had equal with **4g**. Notably, **4g** has better binding energy in the SARS-CoV-2 PL^{Pro} active and allosteric sites than GRL-0617 (Table 2, entry 27) as a SARS-CoV-2 PL^{Pro} inhibitor with IC_{50} of 1.50 ± 0.08 μM [56]. Also, a comparison between binding energies of **4g** and Tropifexor (Table 2, entry 70), which is an efficient repurposed drug for inhibition of SARS-CoV-2 PL^{Pro} (with a IC_{50} of 5.11 ± 1.14 μM and EC_{50} of 4.3 ± 0.5 μM) [57], the results related to the PL^{Pro} active site were so closed and for the PL^{Pro} allosteric site, the compound **4g** was better one.

3. Experimental section

3.1. Reagents, samples, and apparatus in the novel furo[2,3-d] pyrimidines (4a–n) synthesis

1,3-Dimethylbarbituric acid (**2**), and alkyl(viz. cyclohexyl or *tert*-butyl)isocyanides (**3a** or **3b**), and catalysts were commercially available (purchased from Merck, Sigma-Aldrich, and Fluka companies) and used directly without further purification. Aryl(or heteroaryl)glyoxal monohydrates (**1a–g**) were prepared through the Riley oxidation of related aryl(or heteroaryl) methyl ketones using SeO_2 in dioxane:water mixture solvent, in which the amount of water is genuinely trivial compared to dioxane [42b]. Melting points were determined on an Electrothermal 9200 apparatus. Fourier transform infrared (FT-IR) spectra were recorded on a PerkinElmer Spectrum Two FT-IR spectrophotometer, measured as potassium bromide (KBr) disks. ^{1}H and $^{13}C\{H\}$ NMR spectra were recorded on a Bruker Avance 300 MHz spectrometer at 300 MHz and 75 MHz, respectively. Chemical shifts were measured in $CDCl_3$ as solvent relative to tetrametylsilane (TMS) as the internal standard. Elemental analyses were performed using a Leco Analyzer 932.

3.2. General procedure for the one-pot three-component synthesis of 5-aroyl(or heteroaroyl)-6-(alkylamino)-1,3-dimethylfuro[2,3-d]pyrimidine-2,4(1H,3H)-diones (4a–n)

In a round-bottom flask (10 mL) equipped with a magnetic stirrer, a mixture of related aryl(or heteroaryl)glyoxal monohydrate (1 mmol), 1,3-dimethylbarbituric acid (1 mmol), and $ZrOCl_2 \bullet 8H_2O$ (2 mol%, 6.4 mg) in the water solvent (5 mL) was prepared and stirred at 50 ℃ for an appropriate time. After the formation of 1,3-dimethyl-5-(2-oxo-2-aryl (or heteroaryl)ethylidene)pyrimidine-2,4,6(1*H*,3*H*,5*H*)-trione intermediate, intended alkylisocyanide (1 mmol) was added to the reaction environment. After compilation of the reaction, the obtained solid product was filtered and washed with hot ethanol (5 mL) to afford the desired pure furo[2,3-*d*]pyrimidine heterocyclic product.

3.2.1. Physicochemical properties and spectroscopic data of the novel furo [2,3-d]pyrimidines (4a–n)

3.2.1.1. 5-Benzoyl-6-(cyclohexylamino)-1,3-dimethylfuro[2,3-d]pyrimidine-2,4(1H,3H)-dione (4a). Yellow solid; mp 191–192 ℃; FT-IR (KBr) υ_{max} 3412, 3351, 3285, 3089, 3060, 3027, 2937, 2867, 1712, 1624, 1601, 1504, 1492, 1457, 1352, 1305, 1185, 1058, 963, 808, 736, 591, 517, 456 cm^{-1}; ^{1}H NMR (300 MHz, $CDCl_3$) δ_H 8.61 (d, $J = 8.3$ Hz, 1H, —NH—), 7.62 (d, $J = 6.9$ Hz, 2H, Ph—H), 7.51 (t, $J = 7.3$ Hz, 1H, Ph—H), 7.40 (t, $J = 7.5$ Hz, 2H, Ph—H), 3.81–3.70 (m, 1H, N—$CH_{cyclohexyl}$), 3.58 (s, 3H, N—CH_3), 3.29 (s, 3H, N—CH_3), 2.11–2.00 (m, 2H, —CH_2—),

1.87–1.77 (m, 2H, —CH_2—), 1.71–1.58 (m, 2H, —CH_2—), 1.51–1.41 (m, 4H, 2 × —CH_2—); $^{13}C\{^1H\}$ NMR (75 MHz, $CDCl_3$) δ_C 189.20, 161.09, 156.56, 149.97, 148.90, 140.39, 131.15, 128.46, 127.33, 94.40, 92.55, 51.91, 33.43, 29.64, 28.69, 25.24, 24.34; Anal. Calcd for $C_{21}H_{23}N_3O_4$: C, 66.13; H, 6.08; N, 11.02. Found: C, 66.18, H, 6.10; N, 11.12.

*3.2.1.2. 5-(4-Bromobenzoyl)-6-(cyclohexylamino)-1,3-dimethylfuro[2,3-d]pyrimidine-2,4(1H,3H)-dione (**4b**).* Yellow solid; mp 180–181 ℃; FT-IR (KBr) υ_{max} 3518, 3269, 2934, 2859, 1707, 1674, 1650, 1624, 1589, 1573, 1509, 1487, 1455, 1300, 1173, 965, 747, 519, 455 cm^{-1}; ^1H NMR (300 MHz, $CDCl_3$) δ_H 8.65 (d, $J = 8.3$ Hz, 1H, —NH—), 7.53 (d, $J = 8.3$ Hz, 2H, Ph—H), 7.49 (d, $J = 8.7$ Hz, 2H, Ph—H), 3.79–3.71 (m, 1H, N—$CH_{cyclohexyl}$), 3.58 (s, 3H, N—CH_3), 3.31 (s, 3H, N—CH_3), 2.11–1.99 (m, 2H, —CH_2—), 1.89–1.77 (m, 2H, —CH_2—), 1.61–1.27 (m, 6H, 3 × —CH_2—); $^{13}C\{^1H\}$ NMR (75 MHz, $CDCl_3$) δ_C 187.64, 161.31, 156.64, 149.89, 149.01, 139.10, 130.56, 130.17, 125.77, 94.14, 92.28, 51.96, 33.40, 29.69, 28.70, 25.20, 24.33; Anal. Calcd for $C_{21}H_{22}BrN_3O_4$: C, 54.79; H, 4.82; N, 9.13. Found: C, 54.83, H, 4.76; N, 9.18.

*3.2.1.3. 5-(4-Chlorobenzoyl)-6-(cyclohexylamino)-1,3-dimethylfuro[2,3-d]pyrimidine-2,4(1H,3H)-dione (**4c**).* Yellow solid; mp 187–188 ℃; FT-IR (KBr) υ_{max} 3686, 3523, 3277, 2930, 2856, 1714, 1671, 1625, 1542, 1506, 1490, 1454, 1308, 1180, 1090, 964, 845, 747, 513, 459 cm^{-1}; ^1H NMR (300 MHz, $CDCl_3$) δ_H 8.65 (d, $J = 8.3$ Hz, 1H, —NH—), 7.57 (d, $J = 8.2$ Hz, 2H, Ph—H), 7.37 (d, $J = 7.8$ Hz, 2H, Ph—H), 3.79–3.70 (m, 1H, N—$CH_{cyclohexyl}$), 3.59 (s, 3H, N—CH_3), 3.31 (s, 3H, N—CH_3), 2.10–2.01 (m, 2H, —CH_2—), 1.89–1.79 (m, 2H, —CH_2—), 1.57–1.30 (m, 6H, 3 × —CH_2—); $^{13}C\{^1H\}$ NMR (75 MHz, $CDCl_3$) δ_C 187.59, 161.29, 156.65, 149.89, 149.00, 138.66, 137.18, 129.99, 127.64, 94.17, 92.31, 51.96, 33.41, 29.68, 28.69, 25.20, 24.33; Anal. Calcd for $C_{21}H_{22}ClN_3O_4$: C, 60.65; H, 5.33; N, 10.10. Found: C, 60.67, H, 5.30; N, 10.14.

*3.2.1.4. 5-(4-Fluorobenzoyl)-6-(cyclohexylamino)-1,3-dimethylfuro[2,3-d]pyrimidine-2,4(1H,3H)-dione (**4d**).* Yellow solid; mp 174–175 ℃; FT-IR (KBr) υ_{max} 3682, 3510, 3293, 3080, 2938, 2867, 1712, 1671, 1626, 1600, 1547, 1507, 1460, 1222, 1152, 967, 845, 747, 619, 517, 464 cm^{-1}; ^1H NMR (300 MHz, $CDCl_3$) δ_H 8.59 (d, $J = 8.3$ Hz, 1H, —NH—), 7.69–7.58 (m, 2H, Ph—H), 7.14–7.00 (m, 2H, Ph—H), 3.77–3.69 (m, 1H, N—$CH_{cyclohexyl}$), 3.59 (s, 3H, N—CH_3), 3.31 (s, 3H, N—CH_3), 2.11–1.99 (m, 2H, —CH_2—), 1.87–1.77 (m, 2H, —CH_2—), 1.60–1.28 (m, 6H, 3 × —CH_2—); $^{13}C\{^1H\}$ NMR (75 MHz, $CDCl_3$) δ_C 187.60, 166.22, 161.19, 156.70, 149.90, 149.01, 136.47, 130.87, 114.56, 114.26, 94.25, 92.28, 51.94, 33.42, 29.68, 28.69, 25.22, 24.33; Anal. Calcd for $C_{21}H_{22}FN_3O_4$: C, 63.15; H, 5.55; N, 10.52. Found: C, 63.14, H, 5.51; N, 10.55.

*3.2.1.5. 5-(3-Bromobenzoyl)-6-(cyclohexylamino)-1,3-dimethylfuro[2,3-d]pyrimidine-2,4(1H,3H)-dione (**4e**).* Yellow solid; mp 179–180 ℃; FT-IR (KBr) υ_{max} 3421, 3355 3285, 3166, 3064, 2932, 2856, 1717, 1677, 1625, 1569, 1546, 1505, 1477, 1451, 1307, 1259, 1176, 1149, 1047, 964, 894, 754, 716, 605, 521 cm^{-1}; ^1H NMR (300 MHz, $CDCl_3$) δ_H 8.66 (d, $J = 8.3$ Hz, 1H, —NH—), 7.73 (s, 1H, Ph—H), 7.61 (d, $J = 7.8$ Hz, 1H, Ph—H), 7.53 (d, $J = 7.8$ Hz, 1H, Ph—H), 7.29 (t, $J = 7.5$ Hz, 1H, Ph—H), 3.83–3.73 (m, 1H, N—$CH_{cyclohexyl}$), 3.58 (s, 3H, N—CH_3), 3.31 (s, 3H, N—CH_3), 2.10–2.02 (m, 2H, —CH_2—), 1.84–1.78 (m, 2H, —CH_2—), 1.72–1.63 (m, 2H, —CH_2—), 1.51–1.42 (m, 4H, 2 × —CH_2—); $^{13}C\{^1H\}$ NMR (75 MHz, $CDCl_3$) δ_C 187.14, 161.30, 156.57, 149.90, 149.02, 142.13, 133.85, 131.14, 128.88, 127.02, 121.49, 94.07, 92.36, 51.97, 33.37, 29.69, 28.70, 25.20, 24.31; Anal. Calcd for $C_{21}H_{22}BrN_3O_4$: C, 54.79; H, 4.82; N, 9.13. Found: C, 54.73, H, 4.80; N, 9.10.

*3.2.1.6. 5-(4-Hydroxy-3-methoxybenzoyl)-6-(cyclohexylamino)-1,3-dimethylfuro[2,3-d]pyrimidine-2,4(1H,3H)-dione (**4f**).* Yellow solid; mp 187–189 ℃; FT-IR (KBr) υ_{max} 3392, 3162, 3072, 2928, 2855, 1712, 1669, 1605, 1509, 1488, 1467, 1429, 1386, 1355, 1307, 1299, 1283, 1181, 907, 829, 778, 755, 654, 603, 517, 504 cm^{-1}; ^1H NMR (300 MHz, $CDCl_3$) δ_H 8.40 (d, $J = 8.3$ Hz, 1H, —NH—), 7.28 (s, 1H, Ph—H), 7.21 (d, $J = 8.1$ Hz, 1H, Ph—H), 6.88 (d, $J = 8.2$ Hz, 1H, Ph—H), 6.23 (bs, 1H, Ph—OH), 3.89 (s, 3H, Ph—O—CH_3), 3.77–3.70 (m, 1H, N—$CH_{cyclohexyl}$), 3.58 (s, 3H, N—CH_3), 3.31 (s, 3H, N—CH_3), 2.04–1.99 (m, 2H, —CH_2—), 1.83–1.79 (m, 2H, —CH_2—), 1.48–1.40 (m, 6H, 3 × —CH_2—); $^{13}C\{^1H\}$ NMR (75 MHz, $CDCl_3$) δ_C 187.74, 162.34, 160.97, 156.70, 149.95, 148.96, 145.73, 132.27, 124.09, 113.07, 111.22, 92.20, 90.41, 58.85, 51.88, 33.44, 29.65, 28.67, 25.24, 24.31; Anal. Calcd for $C_{22}H_{25}N_3O_6$: C, 61.82; H, 5.90; N, 9.83. Found: C, 61.85, H, 5.87; N, 9.80.

*3.2.1.7. 5-(3,4-Methylendioxybenzoyl)-6-(cyclohexylamino)-1,3-dimethylfuro[2,3-d]pyrimidine-2,4(1H,3H)-dione (**4g**).* Yellow solid; mp 179–180 ℃; FT-IR (KBr) υ_{max} 3678, 3523, 3273, 3166, 3084, 2934, 2855, 2781, 1709, 1675, 1627, 1505, 1491, 1452, 1350, 1307, 1281, 1258, 1246, 1166, 1094, 1040, 967, 931, 856, 821, 767, 748, 669, 521, 494 cm^{-1}; ^1H NMR (300 MHz, $CDCl_3$) δ_H 8.66 (d, $J = 8.3$ Hz, 1H, —NH—), 7.73 (s, 1H, Ph—H), 7.61 (d, $J = 7.9$ Hz, 1H, Ph—H), 7.29 (d, $J = 7.9$ Hz, 1H, Ph—H), 6.03 (s, 2H, O—CH_2—O), 3.81–3.74 (m, 1H, N—$CH_{cyclohexyl}$), 3.59 (s, 3H, N—CH_3), 3.31 (s, 3H, N—CH_3), 2.08–2.02 (m, 2H, —CH_2—), 1.85–1.80 (m, 2H, —CH_2—), 1.51–1.39 (m, 6H, 3 × —CH_2—); $^{13}C\{^1H\}$ NMR (75 MHz, $CDCl_3$) δ_C 187.15, 162.33, 161.30, 156.57, 149.90, 149.01, 142.13, 131.51, 128.89, 127.01, 121.49, 103.00, 94.07, 92.36, 51.98, 33.37, 29.69, 28.70, 25.21, 24.31; Anal. Calcd for $C_{22}H_{23}N_3O_6$: C, 62.11; H, 5.45; N, 9.88. Found: C, 62.15, H, 5.49; N, 9.90.

*3.2.1.8. 5-Benzoyl-6-(tert-butylamino)-1,3-dimethylfuro[2,3-d]pyrimidine-2,4(1H,3H)-dione (**4h**).* Yellow solid; mp 179–180 ℃; FT-IR (KBr) υ_{max} 3428, 3363, 3162, 3060, 2962, 2933, 2872, 1718, 1705, 1676, 1660, 1618, 1601, 1490, 1454, 1287, 1226, 1186, 1107, 967, 902, 878, 784, 765, 744, 735, 611, 525, 512, 470 cm^{-1}; ^1H NMR (300 MHz, $CDCl_3$) δ_H 8.85 (s, 1H, —NH—), 7.68–7.60 (m, 2H, Ph—H), 7.18–6.95 (m, 3H, Ph—H), 3.61 (s, 3H, N—CH_3), 3.31 (s, 3H, N—CH_3), 1.53 (s, 9H, 3 × $CH_{3tert\text{-}butyl}$); $^{13}C\{^1H\}$ NMR (75 MHz, $CDCl_3$) δ_C 187.70, 161.38, 156.67, 149.86, 149.26, 136.45, 132.14, 131.00, 129.83, 114.58, 114.29, 93.85, 93.21, 53.58, 30.04, 29.72, 28.69; Anal. Calcd for $C_{19}H_{21}N_3O_4$: C, 64.21; H, 5.96; N, 11.82. Found: C, 64.20, H, 5.93; N, 11.85.

*3.2.1.9. 5-(4-Bromobenzoyl)-6-(tert-butylamino)-1,3-dimethylfuro[2,3-d]pyrimidine-2,4(1H,3H)-dione (**4i**).* Yellow solid; mp 176–178 ℃; FT-IR (KBr) υ_{max} 3539, 3363, 3105, 2978, 2933, 2872, 1715, 1664, 1622, 1586, 1574, 1502, 1485, 1454, 1401, 1370, 1227, 1185, 1012, 960, 933, 908, 857, 774, 755, 743, 669, 588, 532, 513, 483 cm^{-1}; ^1H NMR (300 MHz, $CDCl_3$) δ_H 8.91 (s, 1H, —NH—), 7.52 (d, $J = 8.5$ Hz, 2H, Ph—H), 7.48 (d, $J = 7.8$ Hz, 2H, Ph—H), 3.59 (s, 3H, N—CH_3), 3.30 (s, 3H, N—CH_3), 1.53 (s, 9H, 3 × $CH_{3tert\text{-}butyl}$); $^{13}C\{^1H\}$ NMR (75 MHz, $CDCl_3$) δ_C 187.73, 161.50, 156.61, 149.86, 149.25, 139.08, 130.59, 130.15, 125.82, 93.74, 93.16, 53.63, 30.01, 29.73, 28.69; Anal. Calcd for $C_{19}H_{20}BrN_3O_4$: C, 52.55; H, 4.64; N, 9.68. Found: C, 52.53, H, 4.60; N, 9.65.

*3.2.1.10. 5-(4-Chlorobenzoyl)-6-(tert-butylamino)-1,3-dimethylfuro[2,3-d]pyrimidine-2,4(1H,3H)-dione (**4j**).* Yellow solid; mp 183–184 ℃; FT-IR (KBr) υ_{max} 3539, 3371, 3105, 3080, 2982, 2941, 2870, 1716, 1662, 1622, 1587, 1577, 1502, 1488, 1455, 1402, 1369, 1227, 1184, 1032, 1010, 960, 935, 910, 862, 755, 743, 632, 619, 560, 509, 473 cm^{-1}; ^1H NMR (300 MHz, $CDCl_3$) δ_H 8.91 (s, 1H, —NH—), 7.63–7.45 (m, 2H, Ph—H), 7.42–7.24 (m, 2H, Ph—H), 3.60 (s, 3H, N—CH_3), 3.31 (s, 3H,

N—CH_3), 1.53 (s, 9H, 3 × $CH_{3tert\text{-}butyl}$); $^{13}C\{^1H\}$ NMR (75 MHz, $CDCl_3$) δ_C 187.67, 161.49, 156.63, 149.86, 149.26, 138.65, 137.23, 130.59, 129.98, 127.66, 93.77, 93.20, 53.63, 30.02, 29.73, 28.70; Anal. Calcd for $C_{19}H_{20}ClN_3O_4$: C, 58.54; H, 5.17; N, 10.78. Found: C, 58.51, H, 5.15; N, 10.75.

*3.2.1.11. 5-(4-Fluorobenzoyl)-6-(tert-butylamino)-1,3-dimethylfuro[2,3-d]pyrimidine-2,4(1H,3H)-dione (**4k**).* Yellow solid; mp 178–179 ℃; FT-IR (KBr) υ_{max} 3419, 3351, 3072, 2978, 2965, 2943, 2880, 1718, 1704, 1675, 1656, 1618, 1602, 1547, 1503, 1461, 1448, 1225, 1186, 1161, 1083, 1054, 973, 921, 849, 778, 758, 745, 619, 517, 478 cm^{-1}; ^1H NMR (300 MHz, $CDCl_3$) δ_H 8.85 (s, 1H, —NH—), 7.70–7.59 (m, 2H, Ph—H), 7.13–7.01 (m, 2H, Ph—H), 3.61 (s, 3H, N—CH_3), 3.31 (s, 3H, N—CH_3), 1.52 (s, 9H, 3 × $CH_{3tert\text{-}butyl}$); $^{13}C\{^1H\}$ NMR (75 MHz, $CDCl_3$) δ_C 187.71, 166.26, 161.38, 156.68, 149.87, 149.26, 136.49, 130.96, 114.60, 114.29, 93.86, 93.22, 53.58, 30.04, 29.73, 28.70; Anal. Calcd for $C_{19}H_{20}FN_3O_4$: C, 61.12; H, 5.40; N, 11.25. Found: C, 61.14, H, 5.43; N, 11.24.

*3.2.1.12. 5-(3-Bromobenzoyl)-6-(tert-butylamino)-1,3-dimethylfuro[2,3-d]pyrimidine-2,4(1H,3H)-dione (**4l**).* Yellow solid; mp 179–180 ℃; FT-IR (KBr) υ_{max} 3413, 3351, 3155, 3072, 2982, 2953, 2884, 1718, 1702, 1676, 1659, 1615, 1572, 1546, 1504, 1477, 1451, 1296, 1224, 1185, 1097, 1035, 1001, 986, 941, 849, 753, 740, 700, 651, 632, 608, 525, 512, 472 cm^{-1}; ^1H NMR (300 MHz, $CDCl_3$) δ_H 8.93 (s, 1H, —NH—), 7.73 (s, 1H, Ph—H), 7.62 (d, $J = 7.9$ Hz, 1H, Ph—H), 7.53 (d, $J = 7.8$ Hz, 1H, Ph—H), 7.27 (t, $J = 8.1$ Hz, 1H, Ph—H), 3.61 (s, 3H, N—CH_3), 3.31 (s, 3H, N—CH_3), 1.54 (s, 9H, 3 × $CH_{3tert\text{-}butyl}$); $^{13}C\{^1H\}$ NMR (75 MHz, $CDCl_3$) δ_C 187.23, 161.51, 156.56, 149.87, 149.28, 142.11, 133.90, 131.60, 131.53, 127.01, 121.50, 93.68, 93.22, 53.69, 30.01, 29.74, 28.70; Anal. Calcd for $C_{19}H_{20}BrN_3O_4$: C, 52.55; H, 4.64; N, 9.68. Found: C, 52.57, H, 4.63; N, 9.70.

*3.2.1.13. 5-(4-Hydroxy-3-methoxybenzoyl)-6-(tert-butylamino)-1,3-dimethylfuro[2,3-d]pyrimidine-2,4(1H,3H)-dione (**4m**).* Yellow solid; mp 182–183 ℃; FT-IR (KBr) υ_{max} 3191, 3027, 2986, 2953, 2839, 2789, 1718, 1703, 1661, 1615, 1598, 1492, 1400, 1285, 1249, 1215, 1179, 1124, 1099, 1051, 980, 865, 851, 838, 788, 759, 746, 652, 628, 603, 517, 471 cm^{-1}; ^1H NMR (300 MHz, $CDCl_3$) δ_H 8.62 (s, 1H, —NH—), 7.29 (s, 1H, Ph—H), 7.22 (d, $J = 6.2$ Hz, 1H, Ph—H), 6.88 (d, $J = 8.1$ Hz, 1H, Ph—H), 5.84 (bs, 1H, Ph—OH), 3.90 (s, 3H, Ph—O—CH_3), 3.61 (s, 3H, N—CH_3), 3.33 (s, 3H, N—CH_3), 1.51 (s, 9H, 3 × $CH_{3tert\text{-}butyl}$); $^{13}C\{^1H\}$ NMR (75 MHz, $CDCl_3$) δ_C 187.87, 162.33, 156.69, 149.94, 149.26, 149.01, 145.75, 132.26, 124.16, 113.06, 111.19, 94.25, 93.36, 77.45, 76.92, 76.61, 55.84, 53.46, 30.10, 29.71, 28.67; Anal. Calcd for $C_{20}H_{23}N_3O_6$: C, 59.84; H, 5.78; N, 10.47. Found: C, 59.86, H, 5.80; N, 10.48.

*3.2.1.14. 5-(3,4-Methylendioxybenzoyl)-6-(tert-butylamino)-1,3-dimethylfuro[2,3-d]pyrimidine-2,4(1H,3H)-dione (**4n**).* Yellow solid; mp 177–178 ℃; FT-IR (KBr) υ_{max} 3424, 3359, 3093, 2978, 2958, 2912, 2888,2802, 1720, 1660, 1609, 1547, 1503, 1453, 1288, 1258, 1239, 1185, 1038, 923, 891, 865, 781, 756, 743, 663, 610, 589, 569, 517, 490 cm^{-1}; ^1H NMR (300 MHz, $CDCl_3$) δ_H 8.62 (s, 1H, —NH—), 7.20 (d, $J = 8.0$ Hz, 1H, Ph—H), 7.16 (2, 1H, Ph—H), 6.80 (d, $J = 7.9$ Hz, 1H, Ph—H), 6.02 (s, 2H, O—CH_2—O), 3.60 (s, 3H, N—CH_3), 3.32 (s, 3H, N—CH_3), 1.30 (s, 9H, 3 × N—$CH_{3tert\text{-}butyl}$); $^{13}C\{^1H\}$ NMR (75 MHz, $CDCl_3$) δ_C 187.65, 162.34, 161.12, 156.68, 150.31, 149.92, 149.22, 147.03, 134.43, 124.57, 107.12, 101.42, 94.12, 93.36, 53.49, 30.08, 29.70, 28.70; Anal. Calcd for $C_{20}H_{21}N_3O_6$: C, 60.14; H, 5.30; N, 10.52. Found: C, 60.15, H, 5.33; N, 10.54.

3.3. In silico molecular docking and ADMET

The molecular docking simulation was carried out using AutoDock Vina (version 1.1.2) as an open-source program incorporating UCSF Chimera (version 1.15) as a graphical user interface on Apple MacBook Pro (Retina, 13-inch, Mid-2014, is equipped with a 2.8 GHz dual-core Intel core i5 processor, 8 GB 1600 MHz DDR3 memory, Intel Iris 1536 MB graphics, and 500 GB Apple SSD SM0512F storage.). All 3D desired crystal structures were downloaded from the Protein Databank (https://www.rcsb.org). Before the molecular docking process, the protein structures were cleaned from the non-standard residues and then prepared and minimized in UCSF Chimera. The 2D structures of the newly synthesized furo[2,3-*d*]pyrimidines were generated in ChemBioDraw Ultra (version 14.0.0.117). Conversion of the 2D skeletons to the related 3D structures of the ligands and their energy minimization processes (by the MM2 force field calculation method) was carried out by ChemBio3D Ultra (version 14.0.0.117). Also, structure editing steps (including dock prep and minimize structure) for the 3D ligands were repeated in UCSF Chimera. The 3D structures of medicinal compounds, which are existed in Fig. 8, were downloaded from PubChem (https://pubchem.ncbi.nlm.nih.gov) and ChemSpider (http://www.chemspider.com), and for some cases 2D version was generated from ChemBioDraw Ultra and then converted to the desired 3D format using ChemBio3D Ultra. All the 3D structures of the mentioned medicinal compounds underwent the aforementioned structure editing steps in UCSF Chimera. All the protein–ligand interactions were analyzed in UCSF Chimera and BIOVIA Discovery Studio (version v21.1.0.20298). The 3D figures of the protein–ligand interactions were visualized by UCSF Chimera, and the related 2D projects were drawn by ChemBioDraw Ultra. The *in silico* ADME and toxicity analyses were investigated using SwissADME (http://www.swissadme.ch) and pkCSM (https://biosig.lab.uq.edu.au/pkcsm/prediction), respectively.

4. Conclusions

Here, we described a green and efficient one-pot three-component regioselective synthetic strategy for the preparation of novel 5-aroyl(or heteroaroyl)-6-(alkylamino)-1,3-dimethylfuro[2,3-*d*]pyrimidine-2,4(1*H*,3*H*)-diones (**4a–n**) in good-to-excellent yields, and then demonstrated their satisfactory multi-targeting inhibitory properties against the active site and putative allosteric hotspots of both SARS-CoV-2 M^{Pro} and PL^{Pro} based on molecular docking studies, especially in comparison with various medicinal compounds which used or investigated to fight against COVID-19 to yet. Besides, the drug-likeness properties of the synthesized heterocyclic frameworks (**4a–n**) were predicted using *in silico* ADMET analyses. Furthermore, our studies in this paper showed that the novel series of furo[2,3-*d*]pyrimidines (**4a–n**), especially **4g** as hit one, can be a potential COVID-19 drug candidate. Notably, research to find and develop new and green synthetic strategies for the pharmaceutically interesting heterocyclic frameworks, especially anti-SARS-CoV-2 agents, is currently underway in our research group.

Declaration of Competing Interest

The authors declare that they have no known competing financial interests or personal relationships that could have appeared to influence the work reported in this paper.

Data availability

Data will be made available on request.

Acknowledgment

We are thankful to the Research Council of Urmia University and the Research Council of Payame Noor University for the partial support of this work.

Appendix A. Supplementary data

Supplementary data to this article can be found online at https://doi.org/10.1016/j.bioorg.2023.106390.

References

[1] (a) O.J. Wouters, K.C. Shadlen, M. Salcher-Konrad, A.J. Pollard, Y. Teerawattananon, M. Jit, Challenges in ensuring global access to COVID-19 vaccines: production, affordability, allocation, and deployment, Lancet 397 (2021) 1023–1034;
(b) S.J.R. da Silva, J.C.F. do Nascimento, R.P.G. Mendes, K.M. Guarines, C.T.A. da Silva, P.G. da Silva, J.J.F. de Magalhães, J.R.J. Vigar, A. Silva-Júnior, A. Kohl, K. Pardee, L. Pena, Two years into the COVID-19 pandemic: lessons learned, ACS Infect. Dis. 8 (2022) 1758–1814;
(c) Z. Shang, S.Y. Chan, W.J. Liu, P. Li, W. Huang, Recent insights into emerging coronavirus: SARS-CoV-2, ACS Infect. Dis. 7 (2021) 1369–1388;
(d) A. Nalbandian, K. Sehgal, A. Gupta, M.V. Madhavan, C. McGroder, J. S. Stevens, J.R. Cook, A.S. Nordvig, D. Shalev, T.S. Sehrawat, N. Ahluwalia, B. Bikdeli, D. Dietz, C. Der-Nigoghossian, N. Liyanage-Don, G.F. Rosner, E. J. Bernstein, S. Mohan, A.A. Beckley, D.S. Seres, T.K. Choueiri, N. Uriel, J. C. Ausiello, D. Accili, D.E. Freedberg, M. Baldwin, A. Schwartz, D. Brodie, C. K. Garcia, M.S.V. Elkind, J.M. Connors, J.P. Bilezikian, D.W. Landry, E.Y. Wann, Post-acute COVID-19 syndrome, Nat. Med. 27 (2021) 601–615;
(e) P. Brodin, Immune determinants of COVID-19 disease presentation and severity, Nat. Med. 27 (2021) 28–33;
(f) J.W. Saville, A.M. Berezuk, S.S. Srivastava, S. Subramaniam, Three-Dimensional visualization of viral structure, entry, and replication underlying the spread of SARS-CoV-2, Chem. Rev. 122 (2022) 14066–14084;
(g) B.A. Ahidjo, M.W.C. Loe, Y.L. Ng, C.K. Mok, J.H. Chu, Current perspective of antiviral strategies against COVID-19, ACS Infect. Dis. 6 (2020) 1624–1634;
(h) H.u. Rashid, N. Ahmad, M. Abdalla, K. Khan, M.A.U. Martines, S. Shabana, Molecular docking and dynamic simulations of Cefixime, Etoposide and Nebrodenside A against the pathogenic proteins of SARS-CoV-2, J. Mol. Struct. 1247 (2022) 131296;
(i) A.K. Kabi, M. Pal, R. Gujjarappa, C.C. Malakar, M. Roy, Overview of Hydroxychloroquine and Remdesivir on severe acute respiratory syndrome coronavirus 2 (SARS-CoV-2), J. Heterocycl. Chem 60 (2023) 165–182;
(j) S. Ponnampalli, N.V.S. Birudukota, A. Kamal, COVID-19: Vaccines and therapeutics, Bioorg. Med. Chem. Lett. 75 (2022) 128987;
(k) C.B. Jackson, M. Farzan, B. Chen, H. Choe, Mechanisms of SARS-CoV-2 entry into cells, Nat. Rev. Cell Biol. 23 (2022) 3–20;
(l) B. Malone, N. Urakova, E.J. Snijder, E.A. Campbell, Structures and functions of coronavirus replication–transcription complexes and their relevance for SARS-CoV-2 drug design, Nat. Rev. Cell Biol. 23 (2022) 21–30;
(m) R. Cannalire, C. Cerchia, A.R. Beccari, F.S. Di Leva, V. Summa, Targeting SARS-CoV-2 proteases and polymerase for COVID-19 treatment: state of the art and future opportunities, J. Med. Chem. 65 (2022) 2716–2746;
(n) S. Xiu, A. Dick, H. Ju, S. Mirzaie, F. Abdi, S. Cocklin, P. Zhan, X. Liu, Inhibitors of SARS-CoV-2 entry: current and future opportunities, J. Med. Chem. 63 (2020) 12256–12274;
(o) R. Chakravarti, R. Singh, A. Ghosh, D. Dey, P. Sharma, R. Velayutham, S. Roy, D. Ghosh, A review on potential of natural products in the management of COVID-19, RSC Adv. 11 (2021) 16711–16735;
(p) L.H. Al-Wahaibi, A. Mostafa, Y.A. Mostafa, O.F. Abou-Ghadir, A. H. Abdelazeem, A.M. Gouda, O. Kutkat, N.M.A. Shama, M. Shehata, H.A. M. Gomaa, M.H. Abdelrahman, F.A.M. Mohamed, X. Gu, M.A. Ali, L. Trembleau, B. G.M. Youssif, Discovery of novel oxazole-based macrocycles as anti-coronaviral agents targeting SARS-CoV-2 main protease, Bioorg. Chem. 116 (2021) 105363;
(q) M. Liu, J. Wang, X. Wan, B. Li, M. Guan, X. Ning, X. Hu, S. Li, S. Liu, G. Song, Discovery and structural optimization of 3-*O*-β-Chacotriosyl betulonic acid saponins as potent fusion inhibitors of Omicron virus infections, Bioorg. Chem. 131 (2023) 106316;
(r) W. Hu, X. Zhang, Y. Liu, T. Liu, J. Wen, X. Peng, X. Xie, W. Chen, Two-stage one-pot synthetic strategy for the key triazone-triazole intermediate of ensitrelvir (S217622), an oral clinical candidate for treating COVID-19, RSC Adv. 12 (2022) 34808–34814;
(s) A. Adel, M.S. Elnaggar, A. Albohy, A.A. Elrashedy, A. Mostafa, O. Kutkat, U. R. Abdelmohsen, E. Al-Sayed, M.A. Rabeh, Evaluation of antiviral activity of Carica papaya leaves against SARS-CoV-2 assisted by metabolomic profiling, RSC Adv. 12 (2022) 32844–32852;
(t) B.S.A.S. Santos, J.L.R. Cunha, I.C. Carvalho, J.M.C. Costa, B.C. Longo, G.C. F. Galinari, P.H.S.M. Diniz, G.M.M. Mendes, F.G. Fonseca, J.S. Abrahão, A.A. P. Mansur, M.F. Leite, R.L. Oréfice, Z.I.P. Lobato, H.S. Mansur, Nanotechnology meets immunology towards a rapid diagnosis solution: the COVID-19 outbreak challenge, RSC Adv. 12 (2022) 31711–31728;
(u) R. Kerkour, N. Chafai, O. Moumeni, S. Chafa, Novel α-aminophosphonate derivates synthesis, theoretical calculation, molecular docking, and in silico prediction of potential inhibition of SARS-CoV-2, J. Mol. Struct. 1272 (2023) 134196;
(v) P. Malik, S. Jain, P. Jain, J. Kumawat, J. Dwivedi, D. Kishore, A comprehensive update on the structure and synthesis of potential drug targets for combating the coronavirus pandemic caused by SARS-CoV-2, Arch. Pharm. 355 (2022) 2100382;
(w) P.F.N. Souza, F.P. Mesquita, J.L. Amaral, P.G.C. Landim, K.R.P. Lima, M. B. Costa, I.R. Farias, M.O. Belém, Y.O. Pinto, H.H.T. Moreira, I.C.L. Magalhaes, D.S. C.M. Castelo-Branco, R.C. Montenegro, C.R. de Andrade, The spike glycoprotein of SARS-CoV-2: a review of how mutations of spike glycoproteins have driven the emergence of variants with high transmissibility and immune escape, Int. J. Bio. Macromol. 208 (2022) 105–125;
(x) M.D. Sacco, C. Ma, P. Lagarias, A. Gao, J.A. Townsend, X. Meng, P. Dube, X. Zhang, Y. Hu, N. Kitamura, B. Hurst, B. Tarbet, M.T. Marty, A. Kolocouris, Y. Xiang, Y. Chen, J. Wang, Structure and inhibition of the SARS-CoV-2 main protease reveal strategy for developing dual inhibitors against M^{pro} and cathepsin L, Sci. Adv. 6 (2020) eabe0751;
(y) C. Ma, M.D. Sacco, B. Hurst, J.A. Townsend, Y. Hu, T. Szeto, X. Zhang, B. Tarbet, M.T. Marty, Y. Chen, J. Wang, Boceprevir, GC-376, and calpain inhibitors II, XII inhibit SARS-CoV-2 viral replication by targeting the viral main protease, Cell Res. 30 (2020) 678–692.

[2] (a) G. La Monica, A. Bono, A. Lauria, A. Martorana, Targeting SARS-CoV-2 main protease for treatment of COVID-19: covalent inhibitors structure–activity relationship insights and evolution perspectives, J. Med. Chem. 65 (2022) 12500–12534;
(b) S. Huff, I.R. Kummetha, S.K. Tiwari, M.B. Huant, A.E. Clark, S. Wang, W. Bray, D. Smith, A.F. Carlin, M. Endsley, T.M. Rana, Discovery and mechanism of SARS-CoV-2 main protease inhibitors, J. Med. Chem. 65 (2022) 2866–2879;
(c) K. Gao, R. Wang, J. Chen, J.J. Tepe, F. Huang, G.-W. Wei, Perspectives on SARS-CoV-2 main protease inhibitors, J. Med. Chem. 64 (2021) 16922–16955;
(d) Q. Hu, Y. Xiong, G.-H. Zhu, Y.-N. Zhang, Y.-W. Zhang, P. Huang, G.-B. Ge, The SARS-CoV-2 main protease (M^{Pro}): structure, function, and emerging therapies for COVID-19, MedComm 3 (2022) e151;
(e) I. Antonopoulou, E. Sapountzaki, U. Rova, P. Christakopoulos, Inhibition of the main protease of SARS-CoV-2 (M^{Pro}) by repurposing/designing drug-like substances and utilizing nature's toolbox of bioactive compounds, Compout. Struct. Biotech. J. 20 (2022) 1306–1344;
(f) R. Chen, Y. Gao, H. Liu, H. Li, W. Chen, J. Ma, Advances in research on 3C-like protease ($3CL^{Pro}$) inhibitors against SARS-CoV-2 since 2020, RSC Med. Chem. 14 (2023) 9–21;
(g) Z. Jin, X. Du, Y. Xu, Y. Deng, M. Liu, Y. Zhao, B. Zhang, X. Li, L. Zhang, C. Peng, Y. Duan, J. Yu, L. Wang, K. Yang, F. Liu, R. Jiang, X. Yang, T. You, X. Liu, X. Yang, F. Bai, X. Liu, L.W. Guddat, W. Xu, G. Xiao, C. Qin, Z. Shi, H. Jiang, Z. Rao, H. Yang, Structure of M^{Pro} from SARS-CoV-2 and discovery of its inhibitors, Nature 582 (2020) 289–293;
(h) A.M. Malebari, H.E.A. Ahmed, S.K. Ihmaid, A.M. Omar, Y.A. Muhammad, S. S. Althagfan, N. Aljuhani, A.-A.-A.-A. El-Sayed, A.H. Halawa, H.M. El-Tahir, S. A. Turkistani, M. Almaghrabi, A.K.B. Aljohani, A.M. El-Agrody, H.A. Abulkhair, Exploring the dual effect of novel 1,4-diarylpyranopyrazoles as antiviral and anti-inflammatory for the management of SARS-CoV-2 and associated inflammatory symptoms, Bioorg. Chem. 130 (2023) 106255;
(i) R. Wang, G. Zhai, G. Zhu, M. Wang, X. Gong, W. Zhang, G. Ge, H. Chen, L. Chen, Discovery and mechanism of action of Thonzonium bromide from an FDA-approved drug library with potent and broad-spectrum inhibitory activity against main proteases of human coronaviruses, Bioorg. Chem. 130 (2023) 106264;
(j) Y.-S. Xu, J.-Z. Chigan, J.-Q. Li, H.-H. Ding, L.-Y. Sun, L. Liu, Z. Hu, K.-W. Yang, Hydroxamate and thiosemicarbazone: two highly promising scaffolds for the development of SARS-CoV-2 antivirals, Bioorg. Chem. 124 (2022) 105799;
(k) A. Aljuhani, H.E.A. Ahmed, S.K. Ihmaid, A.M. Omar, S.S. Althagfan, Y. M. Alahmadi, I. Ahmad, H. Patel, S. Ahmed, M.A. Almikhlafi, A.M. El-Agrody, M. F. Zayed, S.A. Turkistani, S.H. Abulkhair, M. Almaghrabi, S.A. Salama, A.A. Al-Karmalawy, H.S. Abulkhair, In vitro and computational investigations of novel synthetic carboxamide-linked pyridopyrrolopyrimidines with potent activity as SARS-CoV-2-M^{Pro} inhibitors, RSC Adv. 12 (2022) 26895–26907;
(l) R. Redjemia, M. Berredjem, A. Dekir, M. Ibrahim-Ouali, M. Aissaoui, S. Bouacida, A. Bouzina, R. Bahadi, A convenient synthesis, in silico study and crystal structure of novel sulfamidophosphonates: interaction with SARS-CoV-2, J. Mol. Struct. 1275 (2023) 134602;
(m) S. Gao, K. Sylvester, L. Song, T. Claff, L. Jing, M. Woodson, R.H. Weiße, Y. Cheng, L. Schäkel, M. Petry, M. Gütschow, A.C. Schiedel, N. Sträter, D. Kang, S. Xu, K. Toth, J. Tavis, A.E. Tollefson, C.E. Müller, X. Liu, P. Zhan, Discovery and crystallographic studies of trisubstituted piperazine derivatives as non-covalent SARS-CoV-2 main protease inhibitors with high target specificity and low toxicity, J. Med. Chem. 65 (2022) 13343–13364;
(n) Z. Xia, M. Sacco, Y. Hu, C. Ma, X. Meng, F. Zhang, T. Szeto, Y. Xiang, Y. Chen, J. Wang, Rational design of hybrid SARS-CoV-2 main protease inhibitors guided by the superimposed cocrystal structures with the peptidomimetic inhibitors GC-376, Telaprevir, and Boceprevir, ACS Pharmacol. Transl. Sci. 4 (2021) 1408–1421.

[3] (a) H. Tan, Y. Hu, P. Jadhav, B. Tan, J. Wang, Progress and challenges in targeting the SARS-CoV-2 papain-like protease, J. Med. Chem. 65 (2022) 7561–7580;
(b) M. Valipour, Chalcone-amide, a privileged backbone for the design and development of selective SARS-CoV/SARS-CoV-2 papain-like protease inhibitors, Eur. J. Med. Chem. 240 (2022) 114572;
(c) S. Ullrich, C. Nitsche, SARS-CoV-2 papain-like protease: structure, function and inhibition, ChemBioChem 23 (2022) e202200327;
(d) S.A. Elseginy, M.M. Anwar, In silico analysis of SARS-CoV-2 papain-like protease potential inhibitors, RSC Adv. 11 (2021) 38616–38631;
(e) A.-T. Ton, M. Pandey, J.R. Smith, F. Ban, M. Fernandez, A. Cherkasov, Targeting SARS-CoV-2 papain-like protease in the postvaccine era, Trends Pharmacol. Sci. 43 (2022) 906–919;
(f) A.P. Perlinska, A. Stasiulewicz, M.L. Nguyen, K. Swiderska, M. Zmudzinski, A. W. Maksymiuk, M. Drag, J.I. Sulkowska, Amino acid variants of SARS-CoV-2 papain-like protease have impact on drug binding, Plos Comput. Bio. 18 (2022)

e1010667;
(g) M. Sencanski, V. Perovic, J. Milicevic, T. Todorovic, R. Prodanovic, V. Veljkovic, S. Paessler, S. Glisic, Identification of SARS-CoV-2 papain-like protease (PLpro) inhibitors using combined computational approach, ChemistryOpen 11 (2022) e202100248.

[4] (a) K. Gao, R. Wang, J. Chen, L. Cheng, J. Frishcosy, Y. Huzumi, Y. Qiu, T. Schluckbier, X. Wei, G.-W. Wei, Methodology-centered review of molecular modeling, simulation, and prediction of SARS-CoV-2, Chem. Rev. 122 (2022) 11287–11368;
(b) K. De Paris, S.R. Permar, Routine SARS-CoV-2 vaccination for all children, Immun. Rev. 309 (2022) 90–96.

[5] (a) V.T. Sabe, T. Ntombela, L.A. Jhamba, G.E.M. Maguire, T. Govender, T. Naicker, H.G. Kruger, Current trends in computer aided drug design and a highlight of drugs discovered via computational techniques: a review, Eur. J. Med. Chem. 224 (2021) 113705;
(b) P.B. Cox, R. Gupta, Contemporary computational applications and tools in drug discovery, ACS Med. Chem. Lett. 13 (2022) 1016–1029.

[6] (a) E.N. Muratov, R. Amaro, C.H. Andrade, N. Brown, S. Ekins, D. Fourches, O. Isayev, D. Kozakov, J.L. Medina-Franco, K.M. Merz, T.I. Oprea, V. Poroikov, G. Schneider, M.H. Todd, A. Varnek, D.A. Winkler, A.V. Zakharov, A. Cherkasov, A. Tropsha, A critical overview of computational approaches employed for COVID-19 drug discovery, Chem. Soc. Rev. 50 (2021) 9121–9151;
(b) Y. Liu, J. Gan, R. Wang, X. Yang, Z. Xiao, Y. Cao, DrugDevCovid19: an atlas of anti-COVID-19 compounds derived by computer-aided drug design, Molecules 27 (2022) 683;
(c) S. Maghsoudi, B. Taghavi Shahraki, F. Rameh, M. Nazarabi, Y. Fatahi, O. Akhavan, M. Rabiee, E. Mostafavi, E.C. Lima, M.R. Saeb, N. Rabiee, A review on computer-aided chemogenomics and drug repositioning for rational COVID-19 drug discovery, Chem. Biol. Drug Des. 100 (2022) 699–721;
(d) P.P. Sharma, M. Bansal, A. Sethi, Poonam, L. Pena, V.K. Goel, M. Grishina, S. Chaturvedi, D. Kumar, B. Rathi, Computational methods directed towards drug repurposing for COVID-19: advantages and limitations, RSC Adv. 11 (2021) 36181–36198;
(e) N.M. Tam, M.Q. Pham, N.X. Ha, P.C. Nam, H.T.T. Phung, Computational estimation of potential inhibitors from known drugs against the main protease of SARS-CoV-2, RSC Adv. 11 (2021) 17478–17486;
(f) F. Ali, S. Alom, A. Shakya, S.K. Ghosh, U.P. Singh, H.R. Bhat, Implication of in silico studies in the search for novel inhibitors against SARS-CoV-2, Arch. Pharm. 355 (2022) 2100360;
(g) M.M. Ghahremanpour, J. Tirado-Rives, M. Deshmukh, J.A. Ippolito, C.-H. Zhang, I.C. de Vaca, M.-E. Liosi, K.S. Anderson, W.L. Jorgensen, Identification of 14 known drugs as inhibitors of the main protease of SARS-CoV-2, ACS Med. Chem. Lett. 11 (2020) 2526–2533;
(h) S. Mahmoudi, M. Mohammadpour Dehkordi, M.H. Asgarshamsi, The effect of various compounds on the COVID mechanisms, from chemical to molecular aspects, Biophys. Chem. 288 (2022) 106824.

[7] (a) H. Mousavi, A comprehensive survey upon diverse and prolific applications of chitosan-based catalytic systems in one-pot multi-component synthesis of heterocyclic rings, Int. J. Bio. Macromol. 186 (2021) 1003–1166;
(b) T.B. Callis, T.R. Garrett, A.P. Montgomery, J.J. Danon, M. Kassiou, Recent scaffold hopping applications in central nervous system drug discovery, J. Med. Chem. 65 (2022) 13483–13504;
(c) W. Hou, H. Xu, Incorporating selenium into heterocycles and natural products—from chemical properties to pharmacological activities, J. Med. Chem. 65 (2022) 4436–4456;
(d) I.J.P. de Esch, D.A. Erlanson, W. Jahnke, C.N. Johnson, L. Walsh, Fragment-to-lead medicinal chemistry publications in 2020, J. Med. Chem. 65 (2022) 84–99;
(e) R.S. Mancini, C.J. Barden, D.F. Weaver, M.A. Reed, Furazans in medicinal chemistry, J. Med. Chem. 64 (2021) 1786–1815;
(f) A. Mermer, T. Keles, Y. Sirin, Recent studies of nitrogen containing heterocyclic compounds as novel antiviral agents: a review, Bioorg. Chem. 114 (2021) 105076;
(g) Wu, Y.-J. Heterocycles and medicine: a survey of the heterocyclic drugs approved by the U.S. FDA from, to present, Prog. Heterocycl. Chem. 24 (2012) 1–53;
(h) G.C. dos Santos, L.M. Martins, B.A. Bregadiolli, V.F. Moreno, L.C. da Silva-Filho, B.H.S.T. da Silva, Heterocyclic compounds as antiviral drugs: synthesis, structure–activity relationship and traditional applications, J. Heterocycl. Chem. 58 (2021) 2226–2260;
(i) M.M. Alam, 1,2,3-Triazole hybrids as anticancer agents: a review, Arch. Pharm. 355 (2022) 2100158;
(j) A. Dorababu, Pharmacological report of recently designed multifunctional coumarin and coumarin–heterocycle derivatives, Arch. Pharm. 355 (2022) 2100345;
(k) R. Gharat, A. Prabhu, M.P. Khambete, Potential of triazines in Alzheimer's disease: a versatile privileged scaffold, Arch. Pharm. 355 (2022) 2100388;
(l) L.-S. Feng, W.-Q. Su, J.-B. Cheng, T. Xiao, H.-Z. Li, D.-A. Chen, Z.-L. Zhang, Benzimidazole hybrids as anticancer drugs: an updated review on anticancer properties, structure–activity relationship, and mechanisms of action (2019–2021), Arch. Pharm. 355 (2022) 2200051;
(m) O.M. Hendawy, A comprehensive review of recent advances in the biological activities of 1,2,4-oxadiazoles, Arch. Pharm. 355 (2022) 2200045;
(n) M.S.A. Hassan, E.M. Ahmed, A.A. El-Malah, A.E. Kassab, Anti-inflammatory activity of pyridazinones: a review, Arch. Pharm. 355 (2022) 2200067;
(o) N. Desai, J. Monapara, A. Jethawa, A. Khedkar, B. Shingate, Oxadiazole: a highly versatile scaffold in drug discovery, Arch. Pharm. 355 (2022) 2200123;
(p) S. Yahya, K. Haider, A. Pathak, A. Choudhary, P. Hooda, M. Shafeeq, M.S. Yar, Strategies in synthetic design and structure–activity relationship studies of novel heterocyclic scaffolds as aldose reductase-2 inhibitors, Arch. Pharm. 355 (2022) 2200167;
(q) Y. Hong, Y.-Y. Zhu, Q. He, S.-X. Gu, Indole derivatives as tubulin polymerization inhibitors for the development of promising anticancer agents, Bioorg. Med. Chem. 55 (2022) 116597;
(r) G. Ourvy, Recent applications of seven-membered rings in drug design, Bioorg. Med. Chem. 57 (2022) 116650;
(s) V. Sharma, R. Das, D.K. Mehta, S. Gupta, K.N. Venugopala, R. Mailavaram, A. B. Nair, A.K. Shakya, P.K. Deb, Recent insight into the biological activities and SAR of quinolone derivatives as multifunctional scaffold, Bioorg. Med. Chem. 59 (2022) 116674;
(t) B.C. Das, M.A. Shareef, S. Das, N.K. Nandwana, Y. Das, M. Saito, L.M. Weiss, Boron-containing heterocycles as promising pharmacological agents, Bioorg. Med. Chem. 63 (2022) 116748;
(u) S. De, B. Aamna, R. Sahu, S. Perida, S.K. Behera, A.K. Dan, Seeking heterocyclic scaffolds as antivirals against dengue virus, Eur. J. Med. Chem. 240 (2022) 114576;
(v) V. Finger, M. Kufa, O. Soukup, D. Castagnolo, J. Roh, J. Korabecny, Pyrimidine derivatives with antitubercular activity, Eur. J. Med. Chem. 246 (2023) 114946;
(w) A.A. Bhat, I. Singh, N. Tandon, R. Tandon, Structure activity relationship (SAR) and anticancer activity of pyrrolidine derivatives: recent developments and future prospects (a review), Eur. J. Med. Chem. 246 (2023) 114954;
(x) A. Chaurasiya, C. Sahu, S.K. Wahan, P.A. Chawla, Targeting cancer through recently developed purine clubbed heterocyclic scaffolds: an overview, J. Mol. Struct. 1280 (2023) 134967;
(y) P. Wu, J. Zhao, X. Shen, X. Liang, C. He, L. Yin, F. Xu, H. Li, H. Tang, Research progress on the structure and biological diversities of 2-phenylindole derivatives in recent 20 years, Bioorg. Chem. 132 (2023) 106342.

[8] (a) A. Martin-Kohler, J. Widmer, G. Bold, T. Meyer, U. Séquin, P. Traxler, Furo[2,3-*d*]pyrimidines and oxazolo[5,4-*d*]pyrimidines as inhibitors of receptor tyrosine kinases (RTK), Helv. Chim. Acta 87 (2004) 956–975;
(b) Y.-H. Peng, H.-Y. Shiao, C.-H. Tu, P.-M. Liu, J.-T.-A. Hsu, P.K. Amancha, J.-S. Wu, M.S. Coumar, C.-H. Chen, S.-Y. Wang, W.-H. Lin, H.-Y. Sun, Y.-S. Chao, P.-C. Lyu, H.-P. Hsieh, S.-Y. Wu, Protein kinase inhibitor design by targeting the Asp-Phe-Gly (DFG) motif: the role of the DFG motif in the design of epidermal growth factor receptor inhibitors, J. Med. Chem. 56 (2013) 3889–3903;
(c) S.Y. Lin, Y. Chang Hsu, Y.H. Peng, Y.Y. Ke, W.H. Lin, H.Y. Sun, H.Y. Shiao, F. M. Kuo, P.Y. Chen, T.W. Lien, C.H. Chen, C.Y. Chu, S.Y. Wang, K.C. Yeh, C.P. Chen, T.A. Hsu, S.Y. Wu, T.K. Yeh, C.T. Chen, H.P. Hsieh, Discovery of a furanopyrimidine-based epidermal growth factor receptor inhibitor (DBPR112) as a clinical candidate for the treatment of non-small cell lung cancer, J. Med. Chem. 62 (2019) 10108–10123.

[9] X.Y. Jiao, D.J. Kopecky, J.S. Liu, J.Q. Liu, J.C. Jean, M.G. Cardozo, R. Sharma, N. Walker, H. Wesche, S. Li, E. Farrelly, S.-H. Xiao, Z. Wang, F. Kayser, Synthesis and optimization of substituted furo[2,3-*d*]-pyrimidin-4-amines and 7*H*-pyrrolo [2,3-*d*]pyrimidin-4-amines as ACK1 inhibitors, Bioorg. Med. Chem. Lett. 22 (2012) 6212–6217.

[10] E.F. DiMauro, J. Newcomb, J.J. Nunes, J.E. Bemis, C. Boucher, J.L. Buchanan, W. H. Buckner, A. Cheng, T. Faust, F. Hsieh, X. Huang, J.H. Lee, T.L. Marshall, M. W. Martin, D.C. McGowan, S. Schneider, S.M. Turci, R.D. White, X. Zhu, Discovery of 4-amino-5,6-biaryl-furo[2,3-*d*]pyrimidines as inhibitors of Lck: development of an expedient and divergent synthetic route and preliminary SAR, Bioorg. Med. Chem. Lett. 17 (2007) 2305–2309.

[11] Y. Maeda, M. Nakano, H. Sato, Y. Miyazaki, S.L. Schweiker, J.L. Smith, A. T. Truesdale, 4-Acylamino-6-arylfuro[2,3-*d*]pyrimidines: potent and selective glycogen synthase kinase-3 inhibitors, Bioorg. Med. Chem. Lett. 14 (2004) 3907–3911.

[12] P.A. Harris, D. Bandyopadhyay, S.B. Berger, N. Campobasso, C.A. Capriotti, J. A. Cox, L. Dare, J.N. Finger, S.J. Hoffman, K.M. Kahler, R. Lehr, J.D. Lich, R. Nagilla, R.T. Nolte, M.T. Ouellette, C.S. Pao, M.C. Schaeffer, A. Smallwood, H. H. Sun, B.A. Swift, R.D. Totoritis, P. Ward, R.W. Marquis, J. Bertin, P.J. Gough, Discovery of small molecule RIP1 kinase inhibitors for the treatment of pathologies associated with necroptosis, ACS Med. Chem. Lett. 4 (2013) 1238–1243.

[13] H.-Y. Shiao, M.S. Coumar, C.-W. Chang, Y.-Y. Ke, Y.-H. Chi, C.-Y. Chu, H.-S. Sun, C.-H. Chen, W.-H. Lin, K.-S. Fung, P.-C. Kuo, C.-T. Huang, K.-Y. Chang, C.-T. Lu, J. T.A. Hsu, C.-T. Chen, W.-T. Jiaang, Y.-S. Chao, H.-P. Hsieh, Optimization of ligand and lipophilic efficiency to identify an in vivo active furano-pyrimidine aurora kinase inhibitor, J. Med. Chem. 56 (2013) 5247–5260.

[14] Y. Miyazaki, S. Matsunaga, J. Tang, Y. Maeda, M. Nakano, R.J. Philippe, M. Shibahara, W. Liu, H. Sato, L. Wang, R.T. Nolte, Novel 4-amino-furo[2,3-*d*] pyrimidines as Tie-2 and VEGFR2 dual inhibitors, Bioorg. Med. Chem. Lett. 15 (2005) 2203–2207.

[15] A. Gangjee, H.D. Jain, J. Phan, X. Guo, S.F. Queener, R.L. Kisliuk, 2,4-Diamino-5-methyl-6-substituted arylthio-furo[2,3-*d*]pyrimidines as novel classical and nonclassical antifolates as potential dual thymidylate synthase and dihydrofolate reductase inhibitors, Bioorg. Med. Chem. 18 (2010) 953–961.

[16] A. Gangjee, Y. Zeng, J.J. McGuire, R.L. Kisliuk, Synthesis of classical, four-carbon bridged 5-substituted furo[2,3-*d*]pyrimidine and 6-substituted pyrrolo[2,3-*d*] pyrimidine analogues as antifolates, J. Med. Chem. 48 (2005) 5329–5336.

[17] M.A. Mansour, M.A. Oraby, Z.A. Muhammad, D.S. Lasheen, H.M. Gaber, K.A. M. Abouzid, Identification of novel furo[2,3-*d*]pyrimidine based chalcones as potent anti-breast cancer agents: synthesis, *in vitro* and *in vivo* biological evaluation, RSC Adv. 12 (2022) 8193–8201.

[18] (a) M.A. Aziz, R.A.T. Serya, D.S. Lasheen, K.A.M. Abouzid, Furo[2,3-*d*]pyrimidine based derivatives as kinase inhibitors and anticancer agents, Future J. Pharm. Sci.

2 (2016) 1–8;
(b) A.-E.-E. Mansouri, A. Oubella, K. Dánoun, M. Ahmad, J. Neyts, D. Jochmans, R. Snoeck, G. Andrei, H. Morjani, M. Zahouily, H.B. Lazrek, Discovery of novel furo[2,3-*d*]pyrimidin-2-one–1,3,4-oxadiazole hybrid derivatives as dual antiviral and anticancer agents that induce apoptosis, Arch. Pharm. 354 (2021) 2100146;
(c) R.N. Kumar, Y. Poornachandra, P. Nagender, G. Mallareddy, N.R. Kumar, P. Ranjithreddy, C.G. Kumar, B. Narsaiah, Synthesis of novel trifluoromethyl substituted furo[2,3-*b*]pyridine and pyrido[3',2':4,5]furo[3,2-*d*]pyrimidine derivatives as potential anticancer agents, Eur. J. Med. Chem. 108 (2016) 68–78;
(d) M. Hossam, D.S. Lasheen, N.S.M. Ismail, A. Esmat, A.M. Mansour, A.N. B. Singab, K.A.M. Abouzid, Discovery of anilino-furo[2,3-*d*]pyrimidine derivatives as dual inhibitors of EGFR/HER2 tyrosine kinase and their anticancer activity, Eur. J. Med. Chem. 144 (2018) 330–348;
(e) X. Zhang, S. Raghavan, M. Ihnat, E. Hamel, C. Zammiello, A. Bastian, S. L. Mooberry, A. Gangjee, The design, synthesis and biological evaluation of conformationally restricted 4-substituted-2,6-dimethylfuro[2,3-*d*]pyrimidines as multi-targeted receptor tyrosine kinase and microtubule inhibitors as potential antitumor agents, Bioorg. Med. Chem. 23 (2015) 2408–2423;
(f) M.A. Aziz, R.H.T. Serya, D.S. Lasheen, A.K. Abdel-Aziz, A. Esmat, A. M. Mansour, A.N.B. Singab, K.A.M. Abouzid, Discovery of potent VEGFR-2 inhibitors based on furopyrimidine and thienopyrimidne scaffolds as cancer targeting agents, Sci. Rep. 6 (2016) 24460;
(g) E. Sheikhhosseini, Design and effective synthesis of novel furo[2,3-*d*] pyrimidine derivatives containing ethylene ether spacers, J. Saudi Chem. Soc. 22 (2018) 337–342;
(h) A. Zonouzi, M. Habibi Rezaei, R. Mirzazadeh, M. Rezaei Arjomand, Solvent-free synthesis of halogenated furo[2,3-*d*]pyrimidines and their cytotoxic activity on the T47D breast cancer cell line, Org. Prep. Proced. Int. 52 (2020) 374–380.

[19] (a) J.B. Zimmerman, P.T. Anastas, H.C. Erythropel, W. Leitner, Designing for a green chemistry future, Science 367 (2020) 397–400;
(b) H.C. Erythropel, J.B. Zimmerman, T.M. de Winter, L. Petitjean, F. Melnikov, C. H. Lam, A.W. Lounsbury, K.E. Mellor, N.Z. Janković, Q. Tu, L.N. Pincus, M. M. Falinski, W. Shi, P. Coish, D.L. Plata, P.T. Anastas, The Green ChemisTREE: 20 years after taking root with the 12 principles, Green Chem. 20 (2018) 1929–1961;
(c) T. Keijer, V. Bakker, J.C. Slootweg, Circular chemistry to enable a circular economy, Nat. Chem. 11 (2019) 190–195;
(d) P. Anastas, N. Eghbali, Green Chemistry: principles and practice, Chem. Soc. Rev. 39 (2010) 301–312;
(e) M. Hasanpour Galehban, B. Zeynizadeh, H. Mousavi, Diverse and efficient catalytic applications of new cockscomb flower-like Fe_3O_4@SiO_2@KCC-1@MPTMS@Cu^{II} mesoporous nanocomposite in the environmentally benign reduction and reductive acetylation of nitroarenes and one-pot synthesis of some coumarin compounds, RSC Adv. 12 (2022) 11164–11189;
(f) B. Zeynizadeh, F. Sepehraddin, H. Mousavi, Green and highly efficient strategies for the straightforward reduction of carboxylic acids to alcohols using four different and affordable types of hydrogen donors, Ind. Eng. Chem. Res. 58 (2019) 16379–16388;
(g) H. Mousavi, B. Zeynizadeh, R. Younesi, M. Esmati, Simple and practical synthesis of various new nickel boride-based nanocomposites and their applications for the green and expeditious reduction of nitroarenes to arylamines under wet-solvent-free mechanochemical grinding, Aust. J. Chem. 71 (2018) 595–609.

[20] (a) S. Kar, H. Sanderson, K. Roy, E. Benfenati, J. Leszczynski, Green chemistry in the synthesis of pharmaceuticals, Chem. Rev. 122 (2022) 3637–3710;
(b) J. Becker, C. Manske, S. Randl, Green chemistry and sustainability metrics in the pharmaceutical manufacturing sector, Curr. Opin. Green Sustainable Chem. 33 (2022) 100562;
(c) C. Jimenez-Gonzalez, C. Lund, Green metrics in pharmaceutical development, Curr. Opin. Green Sustainable Chem. 33 (2022) 100564;
(d) S.G. Koenig, C. Bee, A. Borovika, C. Briddell, J. Colberg, G.R. Humphery, M. E. Kopach, I. Martinez, S. Nambiar, S.V. Plummer, S.D. Ribe, F. Roschangar, J. P. Scott, H.F. Sneddon, Green chemistry continuum for a robust and sustainable active pharmaceutical ingredient supply chain, ACS Sustainable Chem. Eng. 7 (2019) 16937–16951;
(e) M.C. Bryan, B. Dillon, L.G. Hamann, G.J. Hughes, M.E. Kopach, E.A. Peterson, M. Pourashraf, I. Raheem, P. Richardson, D. Richter, H.F. Sneddon, Sustainable practices in medicinal chemistry: current state and future directions, J. Med. Chem. 56 (2013) 6007–6021;
(f) B.A. de Marco, B.S. Rechelo, E.G. Tótoli, A.C. Kogawa, H.R.N. Salgado, Evolution of green chemistry and its multidimensional impacts: a review, Saudi Pharm. J. 27 (2019) 1–8;
(g) M.C. Bryan, P.J. Dunn, D. Entwistle, F. Gallou, S.G. Koenig, J.D. Hayler, M. R. Hickey, S. Hughes, M.E. Kopach, G. Moine, P. Richardson, F. Roschangar, A. Steven, F.J. Weiberth, Key Green Chemistry research areas from a pharmaceutical manufacturers' perspective revisited, Green Chem. 20 (2018) 5082–5103;
(h) S.G. Koenig, D.K. Leahy, A.S. Wells, Evaluating the impact of a decade of funding from the green chemistry institute pharmaceutical roundtable, Org. Process Res. Dev. 22 (2018) 1344–1359.

[21] (a) C. Capello, U. Fischer, K. Hungerbühler, What is a green solvent? a comprehensive framework for the environmental assessment of solvents, Green Chem. 9 (2007) 927–934;
(b) D. Prat, J. Hayler, A. Wells, A survey of solvent selection guides, Green Chem. 16 (2014) 4546–4551;
(c) V. Hessel, N.N. Tran, M.R. Asrami, Q.D. Tran, N.V.C. Long, M. Escribà-Gelonch, J.O. Tejada, S. Linke, K. Sunmacher, Sustainability of green solvents–review and perspective, Green Chem. 24 (2022) 410–437;
(d) C.J. Clarke, W.-C. Tu, O. Levers, A. Bröhl, J.P. Hallett, Green and sustainable solvents in chemical processes, Chem. Rev. 118 (2018) 747–800;
(e) F.P. Byrne, S. Jin, G. Paggiola, T.H.M. Petchey, J.H. Clarck, T.J. Farmer, A. J. Hunt, C.R. McElory, J. Sherwood, Tools and techniques for solvent selection: green solvent selection guides, Sustainable Chem. Process. 4 (2016) 7.

[22] (a) R.N. Butler, A.C. Coyne, Water: nature's reaction enforcer—comparative effects for organic synthesis "in-water" and "on-water", Chem. Rev. 110 (2010) 6302–6337;
(b) A. Chanda, V.V. Fokin, Organic synthesis "on water", Chem. Rev. 109 (2009) 725–748;
(c) M.-O. Simon, C.-J. Li, Green chemistry oriented organic synthesis in water, Chem. Soc. Rev. 41 (2012) 1415–1427;
(d) B. Zeynizadeh, H. Mousavi, F. Mohammad Aminzadeh, A hassle-free and cost-effective transfer hydrogenation strategy for the chemoselective reduction of arylnitriles to primary amines through *in situ*-generated $nickel^{II}$ dihydride intermediate in water, J. Mol. Struct. 1255 (2022) 131926;
(e) B. Zeynizadeh, F. Mohammad Aminzadeh, H. Mousavi, Chemoselective reduction of nitroarenes, *N*-acetylation of arylamines, and one-pot reductive acetylation of nitroarenes using carbon-supported palladium catalytic system in water, Res. Chem. Intermed. 47 (2021) 3289–3312;
(f) B. Zeynizadeh, F. Mohammad Aminzadeh, H. Mousavi, Green and convenient protocols for the efficient reduction of nitriles and nitro compounds to corresponding amines with $NaBH_4$ in water catalyzed by magnetically retrievable $CuFe_2O_4$ nanoparticles, Res. Chem. Intermed. 45 (2019) 3329–3357;
(g) B. Zeynizadeh, F. Mohammad Aminzadeh, H. Mousavi, Two different facile and efficient approaches for the synthesis of various *N*-arylacetamides via *N*-acetylation of arylamines and straightforward one-pot reductive acetylation of nitroarenes promoted by recyclable $CuFe_2O_4$ nanoparticles in water, Green Process. Synth. 8 (2019) 742–755.

[23] K. Nikoofar, Z. Khademi, A review on green Lewis acids: zirconium(IV) oxydichloride octahydrate ($ZrOCl_2{\cdot}8H_2O$) and zirconium(IV) tetrachloride ($ZrCl_4$) in organic chemistry, Res. Chem. Intermed. 42 (2016) 3929–3977.

[24] A. Ziyaei Halimehjani, N. Keshavarzi, One-pot three-component route for the synthesis of functionalized 4*H*-chromenes catalyzed by $ZrOCl_2{\cdot}8H_2O$ in water, J. Heterocycl. Chem. 55 (2018) 522–529.

[25] M. Rimaz, J. Khalafy, H. Mousavi, S. Bohlooli, B. Khalili, Two different green catalytic systems for one-pot regioselective and chemoselective synthesis of some pyrimido[4,5-*d*]pyrimidinone derivatives in water, J. Heterocycl. Chem. 54 (2017) 3174–3186.

[26] H.R. Tavakoli, S.M. Moosavi, A. Bazgir, $ZrOCl_2{\cdot}8H_2O$ as an efficient catalyst for the synthesis of dibenzo [*b*,*i*]xanthene-tetraones and fluorescent hydroxyl naphthalene-1,4-diones, Res. Chem. Intermed. 41 (2015) 3041–3046.

[27] L. Han, Z. Zhou, $ZrOCl_2{\cdot}8H_2O$ as an efficient and recyclable catalyst for the one-pot multicomponent synthesis of novel [1,3]oxazino[5,6-*c*]quinolin-5-one derivatives, Appl. Organomet. Chem. 33 (2019) e4755.

[28] H.-Y. Lü, J.-J. Li, Z.-H. Zhang, $ZrOCl_2{\cdot}8H_2O$: a highly efficient catalyst for the synthesis of 1,8-dioxo-octahydroxanthene derivatives under solvent-free conditions, Appl. Organomet. Chem. 23 (2009) 165–169.

[29] H.R. Tavakoli, S.M. Moosavi, A. Bazgir, $ZrOCl_2{\cdot}8H_2O$ as an efficient catalyst for the pseudo four-component synthesis of benzopyranopyrimidines, J. Korean Chem. Soc. 57 (2013) 260–263.

[30] A.R. Moosavi-Zare, M.A. Zolfigol, S. Farahmand, A. Zare, A.R. Pourali, R. Ayazi-Nasrabadi, Synthesis of 2,4,6-triarylpyridines using $ZrOCl_2$ under solvent-free conditions, Synlett 25 (2014) 193–196.

[31] S.N. Darandale, D.N. Pansare, N.A. Mulla, D.B. Shinde, Green synthesis of tetrahydropyrimidine analogues and evaluation of their antimicrobial activity, Bioorg. Med. Chem. Lett. 23 (2013) 2632–2635.

[32] J.N. Sangshetti, S.A.M.K. Ansari, D.B. Shinde, $ZrOCl_2{\cdot}8H_2O$ catalyzed solvent-free synthesis of isobenzofuran-1(3*H*)-ones, Chinese Chem. Lett. 22 (2011) 163–166.

[33] J.N. Sangshetti, N.D. Kokare, S.A. Kotharkar, D.B. Shinde, $ZrOCl_2{\cdot}8H_2O$ catalyzed one-pot synthesis of 2,4,5-triaryl-1*H*-imidazoles and substituted 1,4-di(4,5-diphenylimidazol-yl)benzene, Chinese Chem. Lett. 19 (2008) 762–766.

[34] I. Mohammadpoor-Baltork, A.R. Khosropour, S.F. Hojati, $ZrOCl_2{\cdot}8H_2O$ as an environmentally friendly and recyclable catalyst for the chemoselective synthesis of 2-aryloxazolines and bis-oxazolines under thermal conditions and microwave irradiation, Catal. Commun. 8 (2007) 200–204.

[35] D. Azarifar, D. Sheikh, $ZrOCl_2{\cdot}8H_2O$: an efficient, ecofriendly, and recyclable catalyst for ultrasound-accelerated, one-pot, solvent-free synthesis of 8-aryl-7,8-dihydro-[1,3]dioxolo[4,5-*g*]quinolin-6-(5*H*)-one and 4-aryl-3,4-duhydroquinolin-2(1*H*)-one derivatives, Synth. Commun. 43 (2013) 2517–2526.

[36] F. Shirini, M.A. Zolfigol, E. Mollarazi, $ZrOCl_2{\cdot}8H_2O$ as an efficient reagent for the solvent-free synthesis of 3,4-dihydropyrimidin-2-(1*H*)-ones, Synth. Commun. 36 (2006) 2307–2310.

[37] S. Tasqeeruddin, Y.I. Asiri, S. Shaheen, Zirconium(IV) oxychloride octahydrate ($ZrOCl_2{\cdot}8H_2O$): an efficient catalyst for the one-pot multicomponent synthesis of hexahydroquinoline derivatives under conventional heating and microwave irradiation, Russian J. Org. Chem. 58 (2022) 1008–1014.

[38] M. Rimaz, H. Mousavi, M. Behnam, B. Khalili, A green chemoselective one-pot protocol for expeditious synthesis of symmetric pyranodipyrimidine derivatives using $ZrOCl_2{\cdot}8H_2O$, Curr. Chem. Lett. 5 (2016) 145–154.

[39] M. Rimaz, H. Mousavi, P. Keshavarz, B. Khalili, $ZrOCl_2{\cdot}8H_2O$ as a green and efficient catalyst for the expeditious synthesis of substituted 3-arylpyrimido[4,5-*c*]pyridazines in water, Curr. Chem. Lett. 4 (2015) 159–168.

[40] B. Khalili, F. Sadeghzadeh Darabi, B. Eftekhari-sis, M. Rimaz, Green chemistry: $ZrOCl_2{\cdot}8H_2O$ catalyzed regioselective synthesis of 5-amino-1-aryl-1*H*-tetrazoles from secondary arylcyanamides in water, Monatsh. Chem. 144 (2013) 1569–1572.

[41] (a) B.H. Rostein, S. Zaretsky, V. Rai, A.K. Yudin, Small heterocycles in multicomponent reactions, Chem. Rev. 114 (2014) 8323–8359;
(b) A. Dömling, W. Wang, K. Wang, Chemistry and biology of multicomponent reactions, Chem. Rev. 112 (2012) 3083–3135;
(c) F. Sutanto, S. Shaabani, C.G. Neochoritis, T. Zarganes-Tzitzikas, P. Patil, E. Ghonchepour, A. Dömling, Multicomponent reaction–derived covalent inhibitor space, Sci. Adv. 7 (2021) eabd9307;
(d) D. Hurtado-Rodríguez, A. Salinas-Torres, H. Rojas, D. Becerra, J.-C. Castillo, Bioactive 2-pyridone-containing heterocycle syntheses using multicomponent reactions, RSC Adv. 12 (2022) 35158–35176.

[42] (a) B. Eftekhari-Sis, M. Zirak, A. Akbari, Arylglyoxals in synthesis of heterocyclic compounds, Chem. Rev. 113 (2013) 2958–3043;
(b) H. Mousavi, A concise and focused overview upon arylglyoxal monohydrates-based one-pot multi-component synthesis of fascinating potentially biologically active pyridazines, J. Mol. Struct. 1251 (2022) 131742;
(c) A. Jana, D. Ali, P. Bhaumick, L.H. Choudhury, $Sc(OTf)_3$-Mediated one-pot synthesis of coumarin-fused furans: a thiol-dependent reaction for the easy access of 2-phenyl-4*H*-furo[3,2-*c*]chromen-4-ones, J. Org. Chem. 87 (2022) 7763–7777;
(d) D. Gapanenok, A. Makhmet, A.A. Peshkov, D. Smirnova, N. Amire, V. A. Peshkov, D. Spiridonova, D. Dar'in, S. Balalaie, M. Krasavin, Multicomponent assembly of trisubstituted imidazoles and their photochemical cyclization into fused polyheterocyclic scaffolds, J. Org. Chem. 87 (2022) 7838–7851;
(e) P. Bhaumick, R. Kumar, S.S. Acharya, T. Parvin, L.H. Choudhury, Multicomponent synthesis of fluorescent thiazole–indole hybrids and thiazole-based novel polymers, J. Org. Chem. 87 (2022) 11399–11413;
(f) S. Yaragorla, D. Arun, Arylation and aryne insertion into C-acylimines: a simple, flexible, and divergent synthesis of C2-aryl indoles, J. Org. Chem. 87 (2022) 14250–14263;
(g) Q.-X. Zi, C.-L. Yang, K. Li, Q. Luo, J. Lin, S.-J. Yan, Multicomponent cascade reaction by metal-free aerobic oxidation for synthesis of highly functionalized 2-amino-4-coumarinyl-5-arylpyrroles, J. Org. Chem. 85 (2020) 327–338;
(h) G. Brahmachari, N. Nayek, I. Karmakar, K. Nurjamal, S.K. Chandra, A. Bhowmick, Series of functionalized 5-(2-arylimidazo[1,2-*a*]pyridin-3-yl) pyrimidine-2,4(1*H*,3*H*)-diones: a water-mediated three-component catalyst-free protocol revisited, J. Org. Chem. 85 (2020) 8405–8414;
(i) V.G. Shtamburg, V.V. Shtamburg, A.A. Anishchenko, A.V. Mazepa, E. B. Rusanov, 3-Alkoxy-1,5-bis(aryl)imidazolidine-2,4-diones, synthesis and structure, J. Mol. Struct. 1264 (2022) 133259;
(j) H.B. Jalani, J.-H. Jeong, *p*-Toluenesulfonic acid catalyzed, isocyanide-free, Groebke– Blackburn-Bienayme (GBB) type multicomponent synthesis of 3-anilino-imdazo[1,2-*a*]pyridines, J. Heterocycl. Chem. 59 (2022) 1266–1271;
(k) M.E. El-Araby, A.M.E. Omar, A single-step synthesis of 1,3,4,6-tetraaryl-5-aryliminopiperazin-2-one, J. Heterocycl. Chem. 58 (2021) 442–449;
(l) S. Asadi, M. Zebarjad, H. Masoudi, H. Mehrabi, Survey reactivity of 2-amino-pyridine and Meldrum's acid in the presence of aryl glyoxals or or aryl aldehydes; ethyl 2-(3-aryl imidazo[1,2-*a*]pyridin-2-yl)acetates versus ethyl 3-aryl-3-(pyridin-2-ylamino)propanoates, Res. Chem. Intermed. 48 (2022) 251–265;
(m) M.B. Yadav, Y.T. Jeong, Construction of novel penta cyclic indolo-furo[3,2-*c*] quinoline and dihydrochromeno-furo[2,3-*b*]indol via sequential annulation strategy, Tetrahedron Lett. 109 (2022) 154158;
(n) M. Rimaz, H. Mousavi, M. Behnam, L. Sarvari, B. Khalili, Fast and convenient synthesis of new symmetric pyrano[2,3-*d*:6,5-*d'*]dipyrimidinones by an organocatalyzed annulation reaction, Curr. Chem. Lett. 6 (2017) 55–68.

[43] (a) J. Xiong, H.-T. He, H.-Y. Yang, Z.-G. Zeng, C.-R. Zhong, H. Shi, M.-L. Ouyang, Y.-Y. Tao, Y.-L. Pang, Y.-H. Zhang, B. Hu, Z.-X. Fu, X.-L. Miao, H.-L. Zhu, G. Yao, Synthesis of 4-tetrazolyl-substituted 3,4-dihydroquinazoline derivatives with anticancer activity via a one-pot sequential Ugi-azide/palladium-catalyzed azide-isocyanide cross-coupling/cyclization reaction, J. Org. Chem. 87 (2022) 9488–9496;
(b) S. Frippiat, C. Sarre, C. Baudequin, C. Hoarau, L. Bischoff, Insights in the synthesis of imidazolones from aldehydes, isocyanides, or oxazolines, J. Org. Chem. 87 (2022) 7464–7473;
(c) B. Zhang, K. Kurpiewska, A. Dömling, Highly stereoselective Ugi/ Pictet–Spengler sequence, J. Org. Chem. 87 (2022) 7085–7096;
(d) M.V. Il'in, A.A. Sysoeva, A.S. Novikov, D.S. Bolotin, Diaryliodoniums as hybrid hydrogen-and halogen-bond-donating organocatalysts for the Groebke–Blackburn–Bienaymé reaction, J. Org. Chem. 87 (2022) 4569–4579;
(e) M.V. Il'in, A.A. Sysoeva, A.S. Novikov, D.S. Bolotin, Sulfonium and selenonium salts as noncovalent organocatalysts for the multicomponent Groebke–Blackburn–Bienaymé reaction, J. Org. Chem. 87 (2022) 10199–10207;
(f) J.S. Sajko, I. Jerić, Synthesis of N^{β}-substituted 1,2-diazetidin-3-ones by the Ugi reaction comprising chiral α-hydrazino acids, J. Org. Chem. 87 (2022) 7076–7084;
(g) B. González-Saiz, I. Carreira-Barral, P. Pertejo, J. Gómez-Ayuso, R. Quesada, M. García-Valverde, One-pot diastereoselective synthesis of pyrrolopiperazine-2,6-diones by a Ugi/nucleophilic substitution/N-acylation sequence, J. Org. Chem. 87 (2022) 9391–9398;
(h) X. Li, Q. Wang, Q. Zheng, K. Kurpiewska, J. Kalinowska-Tluscik, A. Dömling, Access to isoquinolin-2(1*H*)-yl-acetamides and isoindolin-2-yl-acetamides from a common MCR precursor, J. Org. Chem. 87 (2022) 14463–14475;
(i) R. Xu, Z. Wang, Q. Zheng, P. Patil, A. Dömling, A bifurcated multicomponent synthesis approach to polycyclic quinazolinones, J. Org. Chem. 87 (2022) 13023–13033;
(j) A. Shahriari, K. Amiri, A. Nikbakht, F. Rominger, H.R. Bijanzadeh, S. Balalaie, Synthesis of pyrrolidin-5-one-2-carboxamides through cyclization of *N*-substituted-2-alleneamides, J. Org. Chem. 87 (2022) 7778–7785;
(k) S. Ge, Y.-M. Zhu, X.-P. Xu, S.-J. Ji, [4 + 1 + 1] Tandem cyclization reaction involving isocyanides: access to 2-(trifluoromethyl)quinazolin-4(3*H*)-imines, J. Org. Chem. 87 (2022) 3422–3432;
(l) Y. Li, J. Xu, L.-J. He, Y.-F. Luo, J.-P. Meng, D.-Y. Tang, H.-y. Li, Z.-Z. Chen, Z.-G. Xu, Dieckmann condensation of Ugi *N*-acylamino amide product: facile access to functionalized 2,2-disubstituted indolin-3-ones, J. Org. Chem. 87 (2022) 823–834;
(m) X.-H. Meng, X.-C. Xu, Z. Wang, Y.-X. Liang, Y.-L. Zhao, $NaN(SiMe_3)_2$/CsTFA copromoted aminobenzylation/cyclization of 2-isocyanobenzaldehydes with toluene derivatives or benzyl compounds: one-pot access to dihydroquinazolines and quinazolines, J. Org. Chem. 87 (2022) 3156–3166;
(n) Y. Lv, L. Chen, K. Li, X.-H. Yun, S.-J. Yan, Multicomponent cascade reaction of 3-cyanochromones: highly site-selective synthesis of 2-(1*H*-imidazol-1-yl)-4*H*-chromen-4-one derivatives, J. Org. Chem. 87 (2022) 15187–15196;
(o) L.-Q. Liu, Y.-L. Fang, J.-X. Lin, Y.-C. Wang, Aerobic copper-catalyzed four-component reaction of *O*-phenylenediamines, isocyanides, and selenium powder for the assembly of benzo[4,5]imidazo[2,1-*c*][1,2,4]selenadiazol-3-imine derivatives, J. Org. Chem. 87 (2022) 15120–15128;
(p) L. Bao, Y. Liu, J. Peng, Y. Wang, J. Dong, X. Xu, Chemoselective trimerization of isocyanides: de novo synthesis of 2-indole-substituted quinolines and pyridines, Org. Lett. 24 (2022) 105–109;
(q) Q. Zheng, X. Li, K. Kurpiewska, A. Dömling, Synthesis of tunable fluorescent imidazole-fused heterocycle dimers, Org. Lett. 24 (2022) 5014–5017;
(r) R.L. Mohlala, E.M. Coyanis, M.A. Fernandes, M.L. Bode, Catalyst-free synthesis of novel 1,5-benzodiazepines and 3,4-dihydroquinoxalines using isocyanide-based one-pot, three- and four-component reactions, RSC Adv. 11 (2021) 24466–24473;
(s) M.T. Nazeri, A. Shaabani, Synthesis of polysubstituted pyrroles *via* isocyanide-based multicomponent reactions as an effecient synthesis tool, New J. Chem. 45 (2021) 21967–22011;
(t) M. Khodadadi, M. Ghandi, A. Abbasi, One-pot synthesis of novel spirocyclic-dihydropyrazine-2-(1*H*)ones through a Ugi 4-CR/deprotection, J. Heterocycl. Chem. 59 (2022) 686–694;
(u) R. Singh, R. Kumar, M. Kaur, M.T. Patil, S.C. Sahoo, D.B. Salunke, Groebke–Blackburn–Bienaymé multicomponent reaction coupled with unconventional Pictet-Spengler cyclization for the synthesis of imidazo[4,5-*b*] pyridine fused polycyclic heterocycles, J. Heterocycl. Chem. 59 (2022) 1007–1015;
(v) S. Saeedi, A. Rahmati, Z. Chavoshpour-Natanzi, Synthesis of pyrazolo[5',1': 2,3]imidazo[1,5-*c*]quinazolin-6(5*H*)-ones and molecular docking study of their affinity against the COVID-19 main protease, RSC Adv. 12 (2022) 19579–19589;
(w) T. Chen, F. Ye, R. Hu, B.Z. Tang, Multicomponent polymerizations of isocyanides, aldehydes, and 2-aminopyridine toward imidazo[1,2-*a*]pyridine-containing fused heterocyclic polymers, Macromolecules 55 (2022) 8590–8598.

[44] (a) M. Rimaz, H. Mousavi, A one-pot strategy for regioselective synthesis of 6-aryl-3-oxo-2,3-dihydropyridazine-4-carbohydrazides, Turk. J. Chem. 37 (2013) 252–261;
(b) M. Rimaz, Z. Jalalian, H. Mousavi, R.H. Prager, Base organocatalyst mediated annulation of arylglyoxalmonohydrates with 2,4-dihydroxyquinoline to form new pyranodiquinolinones, Tetrahedron Lett. 57 (2016) 105–109;
(c) M. Rimaz, J. Khalafy, H. Mousavi, A green organocatalyzed one-pot protocol for efficient synthesis of new substituted pyrimido[4,5-*d*]pyrimidinones using a Biginelli-like reaction, Res. Chem. Intermed. 42 (2016) 8185–8200;
(d) M. Rimaz, H. Mousavi, L. Nikpey, B. Khalili, Novel and convenient one-pot strategy for regioselective synthesis of new 5-aryl-3-methyl-1-phenyl-1,2-dihydro-7a*H*-pyrazolo[3,4-*c*]pyridazin-7a-ol derivatives, Res. Chem. Intermed. 43 (2017) 3925–3937;
(e) M. Rimaz, B. Khalili, G. Khatyal, H. Mousavi, F. Aali, A simple and efficient diversity-oriented synthesis of new substituted 3-(arylamino)-6,7-dihydro-1*H*-indazol-4(5*H*)-ones by a KOH-assisted one-pot reaction, Aust. J. Chem. 70 (2017) 1274–1284;
(f) M. Rimaz, H. Mousavi, B. Khalili, F. Aali, A green and practical one-pot two-step strategy for the synthesis of symmetric 3,6-diarylpyridazines, J. Chinese Chem. Soc. 65 (2018) 1389–1397;
(g) M. Rimaz, H. Mousavi, B. Khalili, L. Sarvari, One-pot pseudo three-component condensation reaction of arylglyoxal monohydrates with 1-ethyl-2-thioxodihydropyrimidine-4,6(1*H*,5*H*)-dione for the synthesis of new pyrano[2,3-*d*:6,5-*d'*]dipyrimidines as HIV integrase inhibitor-like frameworks using two different environmentally benign catalytic systems, J. Iran. Chem. Soc. 16 (2019) 1687–1701;
(h) M. Rimaz, H. Mousavi, L. Ozzar, B. Khalili, Facile, capable, atom-economical one-pot multicomponent strategy for the direct regioselective synthesis of novel isoxazolo[5,4-*d*]pyrimidines, Res. Chem. Intermed. 45 (2019) 2673–2694;
(i) R. Bakhshi, B. Zeynizadeh, H. Mousavi, Green, rapid, and highly efficient syntheses of α,α'-bis[(aryl or allyl)idene]cycloalkanones and 2-[(aryl or allyl) idene]-1-indanones as potentially biologic compounds via solvent-free microwave-assisted Claisen-Schmidt condensation catalyzed by $MoCl_5$, J. Chinese Chem. Soc. 67 (2020) 623–637;
(j) M. Hasanpour Galehban, B. Zeynizadeh, H. Mousavi, Ni^{II} NPs entrapped within a matrix of L-glutamic acid cross-linked chitosan supported on magnetic carboxylic acid-functionalized multi-walled carbon nanotube: a new and efficient multi-task catalytic system for the green one-pot synthesis of diverse heterocyclic frameworks, RSC Adv. 12 (2022) 16454–16478;
(k) M. Hasanpour Galehban, B. Zeynizadeh, H. Mousavi, Introducing Fe_3O_4@ SiO_2@KCC-1@MPTMS@Cu^{II} catalytic applications for the green one-pot syntheses of 2-aryl(or heteroaryl)-2,3-dihydroquinazolin-4(1*H*)-ones and 9-aryl-3,3,6,6-

tetramethyl-3,4,5,6,7,9-hexahydro-1*H*-xanthene-1,8(2*H*)-diones, J. Mol. Struct. 1271 (2023) 134017.

[45] A. Ebrahim, B.T. Riley, D. Kumaran, B. Andi, M.R. Fuches, S. McSweeney, D. A. Keedy, The temperature-dependent conformational ensemble of SARS-CoV-2 main protease (M^{pro}), IUCrJ 9 (2022) 682–694.

[46] (a) J. Fan, Y. Liu, R. Kong, D. Ni, Z. Yu, S. Lu, J. Zhang, Harnessing reversed allosteric communication: a novel strategy for allosteric drug discovery, J. Med. Chem. 64 (2021) 17728–17743;
(b) B. Han, F.G. Salituro, M.-J. Blanco, Impact of allosteric modulation in drug discovery: innovation in emerging chemical modalities, ACS Med. Chem. Lett. 11 (2020) 1810–1819;
(c) A.F. Abdel-Magid, Allosteric modulators: an emerging concept in drug discovery, ACS Med. Chem. Lett. 6 (2015) 104–107;
(d) D. Ni, Y. Liu, R. Kong, Z. Yu, S. Lu, J. Zhang, Computational elucidation of allosteric communication in proteins for allosteric drug design, Drug. Discov. Today 27 (2022) 2226–2234;
(e) D. Ni, J. Wei, X. He, A.U. Rehman, X. Li, Y. Qui, J. Pu, S. Lu, J. Zhang, Discovery of cryptic allosteric sites using reversed allosteric communication by a combined computational and experimental strategy, Chem. Sci. 12 (2021) 464–476;
(f) Z.W. Tan, W.-V. Tee, F. Samsudin, E. Guarnera, P.J. Bond, I.N. Berezovsky, Allosteric perspective on the mutability and druggability of the SARS-CoV-2 Spike protein, Structure 30 (2022) 590–607.e4;
(g) E. Guarnera, I.N. Berezovsky, Allosteric drugs and mutations: chances, challenges, and necessity, Curr. Opin. Struct. Biol. 62 (2020) 149–157;
(h) D. Ni, Z. Chai, Y. Wang, M. Li, Z. Yu, Y. Liu, S. Lu, J. Zhang, Along the allostery stream: recent advances in computational methods for allosteric drug discovery, WIREs Comput. Mol. Sci. 12 (2022) e1585;
(i) H.R. Kalhor, E. Taghikhani, Probe into the molecular mechanism of ibuprofen interaction with warfarin bound to human serum albumin in comparison to ascorbic and salicylic acids: allosteric inhibition of anticoagulant release, J. Chem. Inf. Model. 61 (2021) 4045–4057;
(j) D.M. Kremer, C.A. Lyssiotis, Targeting allosteric regulation of cancer metabolism, Nat. Chem. Biol. 18 (2022) 441–450;
(k) Ö.T. Bishop, T.M. Musyoka, V. Barozi, Allostery and missense mutations as intermittently linked promising aspects of modern computational drug discovery, J. Mol. Biol. 434 (2022) 167610;
(l) A.J. Faure, J. Domingo, J.M. Schmiedel, C. Hidalgo-Carcedo, G. Diss, B. Lehner, Mapping the energetic and allosteric landscapes of protein binding domains, Nature 604 (2022) 175–183.

[47] (a) S. Günther, P.Y.A. Reinke, Y. Fernández-García, J. Lieske, T.J. Lane, H. M. Ginn, F.H.M. Koua, C. Ehrt, W. Ewert, D. Oberthuer, O. Yefanov, S. Meier, K. Lorenzen, B. Krichel, J.-D. Kopicki, L. Gelisio, W. Brehm, I. Dunkel, B. Seychell, H. Gieseler, B. Norton-Baker, B. Escudero-Pérez, M. Domaracky, S. Saounane, A. Tolstikova, T.A. White, A. Hänle, M. Groessler, H. Fleckenstein, F. Trost, M. Galchenkova, Y. Gevorkov, C. Li, S. Awel, A. Peck, M. Barthelmess, F. Schlünzen, P.L. Xavier, N. Werner, H. Andaleeb, N. Ullah, S. Falke, V. Srinivasan, B.A. França, M. Schwinzer, H. Brognaro, C. Rogers, D. Melo, J.J. Zaitseva-Doyle, J. Knoska, G.E. Peña-Murillo, A. Rahmani Mashhour, V. Hennicke, P. Fischer, J. Hakanpää, J. Meyer, P. Gribbon, B. Ellinger, M. Kuzikov, M. Wolf, A.R. Beccari, G. Bourenkov, D. von Stetten, G. Pompidor, I. Bento, S. Panneerselvam, I. Karpics, T.R. Schneider, M.M. Garcia-Alai, S. Niebling, C. Günther, C. Schmidt, R. Schubert, H. Han, J. Boger, D.C.F. Monteiro, L. Zhang, X. Sun, J. Pletzer-Zelgert, J. Wollenhaupt, C.G. Feiler, M.S. Weiss, E.-C. Schulz, P. Mehrabi, K. Karničar, A. Usenik, J. Loboda, H. Tidow, A. Chari, R. Hilgenfeld, C. Uetrecht, R. Cox, A. Zaliani, T. Beck, M. Rarey, S. Günther, D. Turk, W. Hinrichs, H.N. Chapman, A. A. Pearson, C. Betzel, A. Meents, X-ray screening identifies active site and allosteric inhibitors of SARS-CoV-2 main protease, Science 372 (2021) 642–646;
(b) O.S. Amamuddy, R.A. Boateng, V. Barozi, D.W. Nyamai, Ö. Bishop, Novel dynamic residue network analysis approaches to study allosteric modulation: SARS-CoV-2 MPro and its evolutionary mutations as a case study, Comput. Struct. Biotech. J. 19 (2021) 6431–6455;
(c) L. Alzyoud, M.A. Ghattas, N. Atatreh, Allosteric binding sites of the SARS-CoV-2 main protease: potential targets for broad-spectrum anti-coronavirus agents, Drug Des. Devel. Ther. 16 (2022) 2463–2478;
(d) S.K. Samrat, J. Xu, X. Xie, E. Gianti, H. Chen, J. Zou, J.G. Pattis, K. Elokely, H. Lee, Z. Li, M.L. Klein, P.-Y. Shi, J. Zhou, H. Li, Allosteric inhibitors of the main protease of SARS-CoV-2, Antiviral Res. 205 (2022) 105381;
(e) L. Strömich, N. Wu, M. Barahona, S.N. Yaliraki, Allosteric hotspots in the main protease of SARS-CoV-2, J. Mol. Biol. 434 (2022) 167748;
(f) G. Jiménez-Avalos, A.P. Vargas-Ruiz, N.E. Delgado-Pease, G.E. Olivos-Ramirez, P. Sheen, M. Fernández-Díaz, M. Quiliano, M. Zimic, Comprehensive virtual screening of 4.8 k flavonoids reveals novel insights into allosteric inhibition of SARS-CoV-2 MPro, Sci. Rep. 11 (2021) 15452;
(g) Y. Bram, X. Duan, B.E. Nilsson-Payant, V. Chandar, H. Wu, D. Shore, A. Fajardo, S. Sinha, N. Hassan, H. Weinstein, B.R. TenOever, S. Chen, R. E. Schwartz, Dual-reporter system for real-time monitoring of SARS-CoV-2 main protease activity in live cells enables identification of an allosteric inhibition path, ACS Bio Med Chem Au 2 (2022) 627–641.

[48] V. Srinivasan, H. Brognaro, P.R. Prabhu, E.E. de Souza, S. Günther, P.Y.A. Reinke, T.J. Lane, H. Ginn, H. Han, W. Ewert, J. Sprenger, F.H.M. Koua, S. Falke, N. Werner, H. Andaleeb, N. Ullah, B.A. Franca, M. Wang, A.L.C. Barra, M. Perbandt, M. Schwinzer, C. Schmidt, L. Brings, K. Lorenzen, R. Schubert, R.R. G. Machado, E.D. Candido, D.B.L. Oliveira, E.L. Durigon, S. Niebling, S. Garcia, O. Yefanov, J. Lieske, L. Gelisio, M. Domaracky, P. Middendorf, M. Groessler, F. Trost, M. Galchenkova, A. Rahmani Mashhour, S. Saouane, J. Hakanpää, M. Wolf, M.G. Alai, D. Turk, A.R. Pearson, H.N. Chapman, W. Hinrichs, C. Wrenger, A. Meents, C. Betzel, Antiviral activity of natural phenolic compounds in complex at an allosteric site of SARS-CoV-2 papain-like protease, Commun. Biol. 5 (2022) 805.

[49] (a) H. van de Waterbeemd, E. Gifford, ADMET *in silico* modelling: towards prediction paradise? Nat. Rev. Drug. Discov. 2 (2003) 192–204;
(b) E.V. Feinberg, E. Joshi, V.S. Pande, A.C. Cheng, Improvement in ADMET prediction with multitask deep featurization, J. Med. Chem. 63 (2020) 8835–8848;
(c) C.-Y. Jia, G.-F. Hao, G.-F. Yang, A drug-likeness toolbox facilitates ADMET study in drug discovery, Drug Discov. Today 25 (2020) 248–258;
(d) L.L.G. Ferreira, A.D. Andricopulo, ADMET modeling approaches in drug discovery, Drug Discov. Today 24 (2019) 1157–1165;
(e) L. Guan, H. Yang, Y. Cai, L. Sun, P. Di, W. Li, G. Liu, Y. Tang, ADMET-score – a comprehensive scoring function for evaluation of chemical drug-likeness, Med. Chem. Commun. 10 (2019) 148–157;
(f) S.Q. Pantaleão, P.O. Fernandes, J.E. Gonçalves, V.G. Maltarollo, K.M. Honorio, Recent advances in the prediction of pharmacokinetics properties in drug design studies: a review, ChemMedChem 17 (2022) e202100542.

[50] (a) A. Daina, O. Michielin, V. Zoete, SwissADME: a free web tool to evaluate pharmacokinetics, drug-likeness and medicinal chemistry friendliness of small molecules, Sci. Rep. 7 (2017) 42717;
(b) B. Bakchi, A.D. Krishna, E. Sreecharan, V.B.J. Ganesh, M. Niharika, S. Maharshi, S.B. Puttagunta, D.K. Sigalapalli, R.R. Bhandare, A.B. Shaik, An overview on applications of SwissADME web tool in the design and development of anticancer, antitubercular and antimicrobial agents: a medicinal chemist's perspective, J. Mol. Struct. 1259 (2022) 132712.

[51] Y.C. Martin, A bioavailability score, J. Med. Chem. 48 (2005) 3164–3170.

[52] D.E.V. Pires, T.L. Blundell, D.B. Ascher, pkCSM: Predicting small-molecule pharmacokinetic and toxicity properties using graph-based signatures, J. Med. Chem. 58 (2015) 4066–4072.

[53] Y. Unoh, S. Uehara, K. Nakahara, H. Nobori, Y. Yamatsu, S. Yamamoto, Y. Maruyama, Y. Taoda, K. Kasamatsu, T. Suto, K. Kouki, A. Nakahashi, S. Kawashima, T. Sanaki, S. Toba, K. Uemura, T. Mizutare, S. Ando, M. Sasaki, Y. Orba, H. Sawa, A. Sato, T. Sato, T. Kato, Y. Tachibana, Discovery of S-217622, a noncovalent oral SARS-CoV-2 3CL protease inhibitor clinical candidate for treating COVID-19, J. Med. Chem. 65 (2022) 6499–6512.

[54] (a) B. Halford, The path to Paxlovid, ACS Cent. Sci. 8 (2022) 405–407;
(b) Y.N. Lamb, Nirmatrelvir plus Ritonavir: first approval, Drugs 82 (2022) 585–591;
(c) J.R.A. Kincaid, J.C. Caravez, K.S. Iyer, R.D. Kavthe, N. Fleck, D.H. Aue, B. H. Lipshutz, A sustainable synthesis of the SARS-CoV-2 M^{pro} inhibitor nirmatrelvir, the active ingredient in Paxlovid, Commun. Chem. 4 (2022) 156;
(d) B.A. Cotrim, J.C. Barros, Development and patent synthesis of nirmatrelvir – the main component of the first oral drug against SARS-CoV-2 Paxlovid®, Aust. J. Chem. 75 (2022) 487–491.

[55] G.J. Lockbaum, A.C. Reyes, J.M. Lee, R. Tilvawala, E.A. Nalivaika, A. Ali, K. N. Yilmaz, P.R. Thompson, C.A. Schiffer, Crystal structure of SARS-CoV-2 main protease in complex with the non-covalent inhibitor ML188, Viruses 13 (2021) 174.

[56] D. Shin, R. Mukherjee, D. Grewe, D. Bojkova, K. Baek, A. Bhattacharya, L. Schulz, M. Widera, A.R. Mehdipour, G. Tascher, P.P. Geurink, A. Wilhelm, G.J. van der Heden van Noort, H. Ovaa, S. Müller, K.P. Knobeloch, K. Rajalingam, B. A. Schulman, J. Cinatl, G. Hummer, S. Ciesek, I. Dikic, Papain-like protease regulates SARS-CoV-2 viral spread and innate immunity, Nature 587 (2020) 657–662.

[57] C. Ma, Y. Hu, Y. Wang, J. Choza, J. Wang, Drug-repurposing screening identified Tropifexor as a SARS-CoV-2 papain-like protease inhibitor, ACS Infect. Dis. 8 (2022) 1022–1030.